Wright State University

CORE Scholar

Browse all Theses and Dissertations | Theses and Dissertations

2009

Dose-Dependent Effects of Oxygen on Metabolism in Rat Cortico-Hippocampal Brain Tissue Slices

Jennifer Lynne Hollyfield
Wright State University

Follow this and additional works at: https://corescholar.libraries.wright.edu/etd_all

 Part of the Molecular Biology Commons

Repository Citation

Hollyfield, Jennifer Lynne, "Dose-Dependent Effects of Oxygen on Metabolism in Rat Cortico-Hippocampal Brain Tissue Slices" (2009). *Browse all Theses and Dissertations*. 278.
https://corescholar.libraries.wright.edu/etd_all/278

This Thesis is brought to you for free and open access by the Theses and Dissertations at CORE Scholar. It has been accepted for inclusion in Browse all Theses and Dissertations by an authorized administrator of CORE Scholar. For more information, please contact library-corescholar@wright.edu.

DOSE-DEPENDENT EFFECTS OF OXYGEN ON METABOLISM IN RAT CORTICO-HIPPOCAMPAL BRAIN TISSUE SLICES

A thesis submitted in partial fulfillment
of the requirements for the degree of
Master of Science

By

JENNIFER LYNNE HOLLYFIELD
B.S. Austin Peay State University, 2002

2009
Wright State University

WRIGHT STATE UNIVERSITY

SCHOOL OF GRADUATE STUDIES

March 27, 2009

I HEREBY RECOMMEND THAT THE THESIS PREPARED UNDER MY SUPERVISION BY Jennifer Lynne Hollyfield ENTITLED Dose-dependent Effects of Oxygen on Metabolism in Rat Cortico-hippocampal Brain Tissue Slices BE ACCEPTED IN PARTIAL FULFILLMENT OF THE REQUIREMENTS FOR THE DEGREE OF Master of Science.

Nicholas V. Reo, Ph.D.
Thesis Director

Steven Berberich, Ph.D.
Department Chair

Committee on
Final Examination

Nicholas V. Reo, Ph.D.

Lawrence Prochaska, Ph.D.

John Paietta, Ph.D.

Joseph F. Thomas, Jr., Ph.D.
Dean, School of Graduate Studies

ABSTRACT

Hollyfield, Jennifer Lynne. M.S., Department of Biochemistry and Molecular Biology, Wright State University, 2009. Dose-dependent Effects of Oxygen on Metabolism in Rat Cortico-Hippocampal Brain Tissue Slices.

Studies have shown that 95% oxygen increases neuronal excitability and ROS production. We wanted to investigate the dose-dependent effects of oxygen on brain slice metabolism. We exposed rat brain cortico-hippocampal tissue slices to 0.40, 0.95, and 4.50 ATA O_2 for 60 minutes, made dual-phase tissue extracts, and used multi-nuclear NMR experiments to elucidate the slice metabolism. We found that low doses of oxygen may shift metabolism toward anaerobic glycolysis. Elevated lactate suggests this shift, along with elevated ratios of NAD+/NADH which may drive the reactions toward the production of lactate. The results also suggest that high doses of oxygen may cause aerobic glycolysis and oxidative phosphorylation to accelerate. Lower lactate amounts along with a low NAD+/NADH ratio may be driving these reactions towards pyruvate and the TCA cycle and suggest a highly oxidized environment. The 0.40 ATA O_2 results suggest a hypoxic environment while the 0.95 and 4.50 ATA O_2 results suggest hyperoxic environments that lead to changes in metabolism on both ends of the oxygen spectrum.

TABLE OF CONTENTS

		Page
I.	INTRODUCTION AND PURPOSE.....	1
II.	BACKGROUND AND SIGNIFICANCE	
	a. Oxygen and Oxidative Stress.....	3
	b. Reactive Oxygen Species.....	4
	c. Hippocampus.....	6
	d. Nuclear Magnetic Resonance.....	6
III.	MATERIALS AND MATERIALS	
	a. Materials.....	8
	b. Experimental Protocol.....	8
	c. Chemical Extract Preparation.....	9
	d. Preparation of NMR Samples.....	10
	e. NMR Experiments.....	11
	f. ^{1}H Principle Component Analysis and Linear Discriminant Analyses.....	14
	g. Metabolite Quantitative Analysis.....	16
	h. Statistical Analysis.....	18
IV.	RESULTS	
	a. Correction Factor.....	19
	b. Principle Component Analysis and	

Discriminant Analyses..... 21

c. Metabolite Analyses from ^{1}H Aqueous Spectra... 27

d. Metabolite Analyses from ^{31}P Aqueous Spectra. 29

e. Metabolite Ratios..... 30

f. Metabolite Analyses from ^{31}P Lipid Spectra..... 36

g. Metabolite Analyses from ^{13}C Lipid Spectra..... 37

h. Time Dependence of Metabolite Ratios..... 38

V. Discussion

a. PCA and LDA Analyses..... 39

b. Neuronal Cell Viability..... 39

c. Oxygen Effects on Energy Metabolism..... 39

d. Phospholipid Synthesis and Degradation..... 43

e. Effects of Oxygen on Lipids..... 45

VI. Conclusions..... 47

VII. References..... 49

Appendix A…….. 53

Appendix B…… 56

LIST OF FIGURES

Figure		Page
1.	Dual-phase tissue extracts……..	7
2.	Timeline of experiments……	9
3.	Representative ^{1}H aqueous spectrum from rat cortico-hippocampal brain tissue slices…….	12
4.	Representative ^{31}P aqueous spectrum from rat cortico-hippocampal brain tissue slices…….	13
5.	Representative ^{31}P lipid spectrum from rat cortico-hippocampal brain tissue slices…….	13
6.	Representative ^{13}C lipid spectrum from rat cortico-hippocampal brain tissue slices…….	14
7A.	PCA scores plot from ^{1}H aqueous spectra……..	22
7B.	PCA scores plot from ^{1}H aqueous spectra……..	23
7C.	PCA scores plot from ^{1}H aqueous spectra……..	24
8A.	LDA projection plot from ^{1}H aqueous spectra……	25
8B.	LDA projection plot from ^{1}H aqueous spectra……	26
8C.	LDA projection plot from ^{1}H aqueous spectra……	26
9.	Quantified ^{1}H aqueous metabolites…….	28
10.	Quantified ^{1}H aqueous metabolites…….	29
11.	Quantified ^{31}P aqueous metabolites…….	30

12. Metabolite Ratios from ^{31}P and ^{1}H aqueous spectra…… 31

13. Ratios of G3P/DHAP and lactate/pyruvate plotted per oxygen concentration……. 32

14. Quantified ^{31}P aqueous metabolites……. 33

15. Quantified ^{31}P aqueous metabolites……. 33

16. Metabolite ratios from ^{31}P aqueous spectra……. 34

17. Quantified ^{31}P aqueous metabolites……. 35

18. Quantified ^{31}P lipid metabolites…… 36

19. Quantified ^{13}C lipid metabolites…… 38

20. Glycolytic pathway and TCA cycle affected by 0.40 ATA O_2……... 41

21. Glycolytic pathway and TCA cycle affected by 4.50 ATA O_2……... 43

LIST OF TABLES

Table		Page
I.	Tissue slice weights for each experimental group……..	20
II.	Highest ranked ^{1}H aqueous LDA weighting factors, PPMs, and identified metabolites……..	27
III.	Quantified ^{31}P phospholipids……..	37
IV.	Metabolite analysis from ^{13}C lipid spectra…….	37
V.	Metabolite ratios……..	38

LIST OF ABBREVIATIONS

ATA – Atmospheres absolute

ATP - Adenosine triphosphate

CL – Cardiolipin

DHAP – Dihydroxyacetone phosphate

G3P - Glycerol – 3 phosphate

GPC – Glycerophosphocholine

GPE – Glycerophosphoethanolamine

LDA – Linear discriminant analysis

NAA – N-acetylaspartate

PCA – Principal component analysis

Pcho – Phosphocholine

PCr – Phosphocreatine

PE – Phosphatidylethanolamine

PE pls – Phosphatidylethanolamine plasmalogen

Petn – Phosphoethanolamine

P_i – Inorganic phosphate

PI – Phosphatidylinositol

$PtiO_2$ – Tissue partial pressure of oxygen

ROS – Reactive oxygen species

Chapter I

Introduction and Purpose

Chronic exposure to hypoxia or hyperoxia can yield great amounts of redox stress which can disrupt cellular and metabolic functions. This is applicable in sleep apnea and ischemic reperfusion events such as stroke, heart attack, and hyperbaric oxygen therapy. *In vitro* tissue slice experiments were developed by Henry McIlwain in the 1950s. Slices are sectioned while in an artificial cerebrospinal fluid (aCSF) and perfused with 95% oxygen and 5% CO_2. Slice work has always been done at 95% oxygen so the core would not be anoxic. Recent measurements of tissue slice partial pressures from Dr. Jay Dean's laboratory have shown that, with the advent of thinner tissue slices, even the core is hyperoxic when exposed to 95% oxygen. Electrophysiology experiments conducted in that lab also showed that neurons in the tissue slice have a more rapid firing rate. ROS production is elevated when tissue slices are exposed to 95% O_2.

This research project was developed to determine the dose-dependent effects of oxygen on brain tissue metabolism to correlate with the electrophysiology results and the increase in ROS production results that were found in Dr. Jay Dean's laboratory. This will provide a profile of tissue metabolism and help to better understand the overall effects of O_2 in these tissue slices. No studies have shown the effects of hyperoxia on metabolism or pathways though. This leads to the following hypotheses:

Hypothesis I: High oxygen concentrations will cause a shift toward aerobic glycolysis and oxidative phosphorylation thereby perturbing the natural balance of the slice metabolism.

Hypothesis II: High oxygen concentrations will have a detrimental effect on lipid metabolism and phospholipid synthesis and degradation pathways compared to low oxygen concentrations due to increased ROS production.

Investigation of these hypotheses will be done by:

- Conducting rat brain slice experiments at 0.40, 0.95, and 4.50 ATA oxygen concentrations.
- Extracting metabolites from brain slices using a dual-phase tissue extraction process.
- Performing multi-nuclear NMR experiments on lipid and aqueous extracts.
- Determining differences in small metabolites, phospholipids, and fatty acid and cholesterol lipid molecules between treatment groups.

Chapter II

Background and Significance

A. Oxygen and Oxidative Stress

Oxygen makes up about 21 percent of the air we breathe. It is essential for most organisms to survive. It is thought that the more oxygen there is in the air, the better. Hospitals will administer 100 percent oxygen to a patient when levels in the blood are low. This is at normobaric pressure, whereas high percentages of oxygen are also used when diving and for hyperbaric oxygen therapy (HBOT) but these are in pressurized environments. Oxygen is not thought of as something that is dangerous or could be damaging within living systems. Recent studies have shown otherwise.

The brain tissue partial pressure of oxygen (Pti_{O2}) measured *in vivo* of a mammal breathing room air at or near sea level (1 ATA) on average will range from about 3 Torr to 35 Torr, depending on the area of the brain. [1] This is considered normoxic. Breathing pure O_2 at sea level will cause the brain tissue partial pressure to increase to between 40 to 90 Torr. [2, 3] Hyperoxic is defined as a Pti_{O2} which is greater than 35 Torr and hypoxic is considered less than 3 Torr. Not only is the concentration of oxygen important, but the length of time that the tissue is exposed has an additive effect. The dose of oxygen is defined as the concentration of oxygen times the time exposed.

Tissue slice work began back in the 1950s when Henry McIlwain developed the brain slice preparation. [4] Slice work has since become an accepted technique. But

slice work is conducted with a perfusate bubbled with 95% oxygen (0.95 ATA), which is considerably more than the 21% in ambient air. This is considered normoxic, a control, for slice work and prevents the core of the slice, up to 700 μm thick, from becoming anoxic. [5] It has been shown recently though that slices 300 to 400 um thick that are exposed to 0-15% oxygen renders a Pti_{O2} closer to what is measured in the normoxic intact brain than that in the hypoxic brain. [1] Mulkey *et al*. showed that 95% oxygen causes a Pti_{O2} of 291 Torr even at the core. [6] This is a 10-fold increase over *in vivo* and is hyperoxic. Exposing brain slices to 3.3 ATA, which is a little greater than that used with HBOT, caused the core Pti_{O2} to rise to 1517 Torr, a 50-fold increase.

B. Reactive Oxygen Species

Reactive Oxygen Species (ROS) are molecules or ions that are highly reactive due to unpaired electrons in the valence shell. They are the natural byproduct of oxygen metabolism, but when produced in excess can cause damage to surrounding cells. Superoxide anion, $\bullet O_2^-$, is generated in the mitochodria, but overproduction can occur as a result of mitochondrial dysfunction. [7] It has been shown that when tissue is exposed to hyperoxia that reactive oxygen species production increases [8] [9-12] including superoxide, hydrogen peroxide, hydroxyl radicals, nitric oxide, peroxynitrite, and associated intermediates. [9, 10, 12-16] This results in oxidative stress because the increased amount of ROS may overwhelm antioxidants [17-19] and may have an effect on cellular and metabolic function.

Hyperbaric oxygen therapy (HBOT) also increases ROS production that can result in CNS toxicity, the symptoms of which include seizures, slow heart rate, increased

respiration, and shortness of breath. [20-24] Even hyperoxia at normal pressures has been shown to have effects on neuronal excitability. [25-27] [28] In electrophysiology experiments conducted in rat brain slices, hyperoxia increased the firing rate of neurons in medullary [29] and solitary complex neurons. [6] These effects have been attributed to the oxidative effects of ROS.

A study exposing slices to 95% oxygen under normobaric pressures found a significant increase in compounds derived from the oxidation of docosahexanoic acid and suggested that the slices undergo a severe oxidative insult at this oxygen concentration.[11] In a similar experiment, measurements of $\bullet O_2^-$ in CA1 neurons of rat hippocampal slices with dihydroethidium, which detects intracellular $\bullet O_2^-$ production, have shown that $\bullet O_2^-$ production was significantly increased in slices exposed to 95% O_2 at normobaric pressure as compared to 60, 40, and 20% O_2. [30] That same experiment showed that the most cell death and increased excitability occurred when exposed to 95% O_2 over the lower oxygen levels. Hyperoxia will likely affect metabolism in the slice as well, but this has never been studied directly. This is suggested by another study that compared slices exposed to hyperbaric oxygen with slices that had been metabolically poisoned. [6] The higher the oxygen PO_2 in the tissue the lower the tissue oxygen consumption. This was not different from the PO_2 in tissue that had been metabolically poisoned with 2-deoxy-D glucose. They suggested that high oxygen concentrations appeared to reduce metabolism.

C. Hippocampus

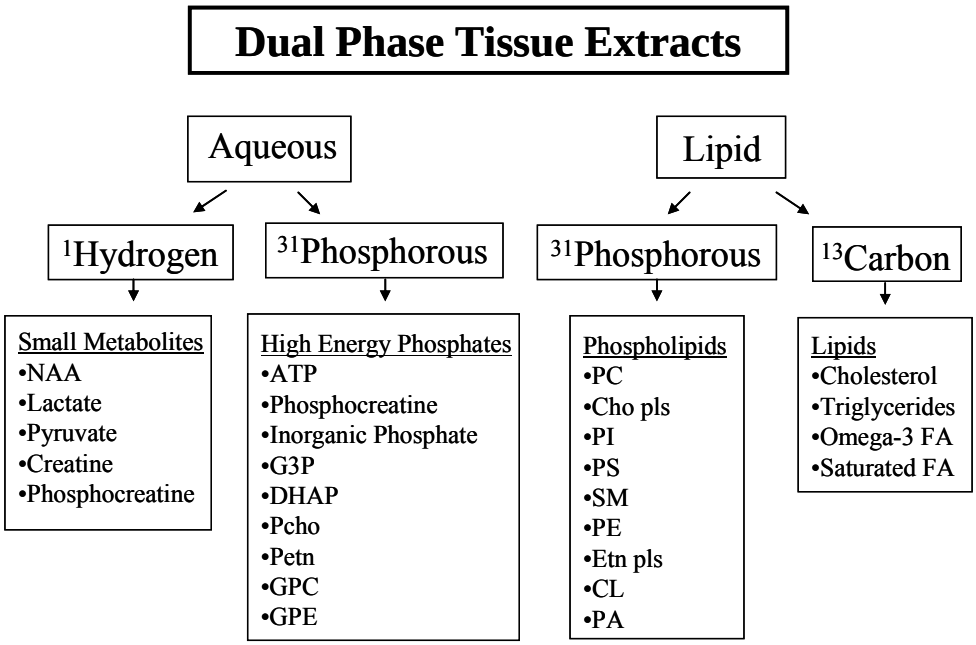
The CA1 region of the hippocampus is highly sensitive to changes in oxygen levels. Hippocampal neurons are thought to play a role in seizure genesis during oxygen toxicity [17, 31] and other seizure-promoting conditions. [31-33] There have been many studies on the effects of hypoxia and anoxia on the electrophysiology of these neurons, but few studies with hyperoxia. [34, 35] [31, 36] It has been shown, though, that with acute exposure to hyperoxia, there is an increased firing rate and increased synaptic activity. [1, 34, 35]

D. Nuclear Magnetic Resonance (NMR)

NMR is a very useful tool in examining changes in metabolic pathways across treatment groups (Figure 1). Many different metabolites involved in glycolysis, energy metabolism, and lipid pathways can be examined in one experiment and amounts determined in tissue extracts. It can examine synthesis and degradation pathways. NMR experiments in our lab have been used to elucidate liver phospholipid biosynthesis with ^{13}C enrichments [37], look at the effects of hepatocarcinogens on liver phospholipid biosynthesis [38], and study phospholipid biosynthesis in brain before and after a toxic insult [39]. Chemical extracts of brain tissue slices can be prepared to separate lipid fractions and aqueous fractions. Metabolic pathways that are affected by different oxygen concentrations can be elucidated by using a multi-nuclear approach of hydrogen (^{1}H), phosphorus (^{31}P) and carbon (^{13}C), analysis of both the lipid and aqueous extracts of the brain tissue slices. Aqueous extracts can reveal changes in energy metabolism by showing ATP levels, phosphocreatine (PCr), and inorganic phosphate (Pi). Also, various

phosphomonoesters including phosphocholine (Pcho) and phosphoethanolamine (Petn) and phosphodiesters (glycerophosphocholine, GPC; and glycerophosphoethanolamine, GPE) that are important in phospholipid synthesis and degradation pathways can be examined. Tissue viability can also be examined by measuring N-acetylaspartate (NAA), which is a neuronal marker. Loss of NAA can show neuronal cell death. [40] Examination of the lipid extracts using ^{31}P NMR can show changes in the phospholipid profile, including phosphatidylcholine and cardiolipin, which is an important mitochondrial membrane lipid. The ^{13}C lipid profile can provide information about free and esterified fatty acids and cholesterol levels and can elucidate changes in lipids, possible signaling pathways or membrane structure. NMR is a useful tool to study the metabolic changes in brain slice tissue extracts to determine dose-dependent effects of oxygen of which has not been investigated.

Figure 1: Dual Phase Tissue Extracts



Chapter III

EXPERIMENTAL PROCEDURES

A. Materials

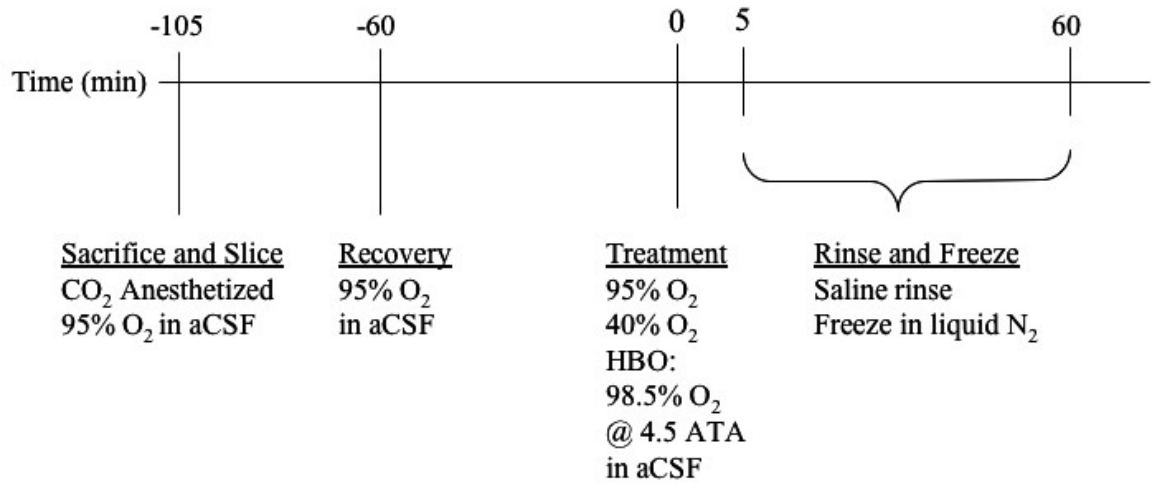
Male Sprague-Dawley rats (40-42 days of age) were obtained from Harlan (Indianapolis, IN) and were housed at 22ºC with a 12-h light/dark cycle. Rats were fed Harlan Teklad 22/5 rodent diet #8640. All chemicals were reagent grade and purchased from standard sources.

B. Experimental Protocol

Figure 2 depicts a timeline of the experimental protocol. Rats were anesthetized using CO_2 followed by decapitation. Hippocampus with surrounding cortices was isolated and 400-µm-thick slices were cut sagittally with a Vibratome (series 1000) sectioning system (average 12 slices per animal). Slices were incubated at room temperature for 1 hour with 95% O_2-5% CO_2 in artificial cerebrospinal fluid (aCSF) composed of (in mM): 5.0 KCl, 124 NaCl, 1.3 $MgSO_4$, 26 $NaHCO_3$, 1.24 KH_2PO_4, 10 Glucose, and 2.4 $CaCl_2$. After this 1 h equilibration period, the slices were transferred to a two-sided perfusion container and placed inside a pressure chamber at 37°C. The perfusion medium consisted of aCSF equilibrated with one of the following gas mixtures for the specified time period: 95% O_2-5% CO_2 for 5 min. (Group 1); 95% O_2-5% CO_2 for 60 min. (Group 2), 40% O_2-5% CO_2 for 60 min. (Group 3), or 98.5% O_2-1.5% CO_2 at

4.5 ATA for 60 min, (hyperbaric oxygen, Group 4). Pressurization for hyperbaric oxygen group was less than 5 minutes; decompression for the same group was at that same rate. At the completion of the experiment, slices were removed from the containers, rinsed in 0.9% saline, gathered into a strainer and blotted dry, then quickly frozen in liquid nitrogen (total time for this procedure was < 1 minute). Tissue slices from 2 animals were combined to constitute 1 sample, with sample weights between 500 and 700 mg, for analysis by NMR. This was determined from preliminary experiments where approximately 24 tissue slices yielded sufficient sample for good signal-to-noise ratio in the various NMR experiments.

Figure 2: Timeline of Experiments.



C. Chemical Extract Preparation

Chemical extracts were prepared using a dual phase extraction method. This method allows for extraction of an aqueous and a lipid phase simultaneously. All solvents and homogenates were kept on ice during the entire procedure. The brain slices were homogenized using a 40-ml glass homogenizer tube and Teflon pestle. Slices were

first homogenized in methanol (MeOH), then chloroform ($CHCL_3$) and water (1:1:1 v/v/v, 0.7ml/100 mg tissue). The homogenate was centrifuged at 2000 X g for 25 minutes. This separated the homogenate into 2 phases and a pellet. The supernatant was then transferred to a separatory funnel through filter paper and the pellet was washed 3 times with 0.5 ml of each extraction solvent, centrifuged for 5 minutes (2000 X g), and transferred to the same separatory funnel through the filter paper. The sample was left to separate completely at 4°C for 17-24 hours.

The sample was moved to room temperature to allow for further separation for 2 hours. The upper phase, containing the aqueous portion, was removed by aspiration into a lyophilizer flask and partially evaporated under a gentle nitrogen gas stream in a 25°C water bath to remove most of the MeOH. The bottom phase containing the lipid was drained into a vial and evaporated to dryness under a gentle nitrogen gas stream in a 25°C water bath. The separatory funnel was washed 3 times with 0.5 ml of each extraction solvent, allowed 45 minutes to separate, and transferred to the appropriate container for evaporation. The aqueous phase was then frozen in the flask with liquid nitrogen and lyophilized to dryness overnight. The lipid phase was placed on a vacuum overnight and weighed the next day to obtain total lipid content. The lipid sample was then stored in 0.6 ml of deuterochloroform ($CDCL_3$) at -15 °C.

D. Preparation of NMR Samples

Dried extracts recovered from the aqueous phase were reconstituted in 2 ml of water with 0.1 g of Chelex 100 (removes divalent cations) and stirred for 2 hours at 4°C. The sample was transferred to a 15 ml disposable centrifuge tube and centrifuged for 10

minutes (2000 X g) at 4°C to remove the Chelex 100. The supernatant was transferred to a vial. The lyophilizer flask was rinsed with 2 ml of water 3 times, centrifuged, and transferred to the vial. The vial was frozen in liquid nitrogen and lyophilized to dryness overnight. The next day, the vial was weighed and the aqueous sample weight calculated. The final dried aqueous extracts were reconstituted in 0.7 ml of deuterium oxide (D_2O, 100%) and 0.603 ml of reconstituted sample transferred to a 5mm NMR tube. A standard of trimethysilylpropionic (2,2,3,3 d_4) acid (TSP; 0.43mM) was added for proton (^1H) NMR. Disodium ethylenediaminetetraacetic acid (Na_2EDTA; 30.5 mM) and methylene diphosphonic acid (MDPA; 1.5 mM), a standard, were added for phosphorus (^{31}P) NMR. The final lipid extracts were prepared by transferring 0.5 ml of lipid sample (in $CDCl_3$ solvent) to a 5mm NMR tube and mixing with 0.2 ml Cs_2 (EDTA) in 1:4 D_2O: MeOH. Carbon (^{13}C) and phosphorus (^{31}P) NMR spectra were then acquired.

E. NMR Experiments

High-resolution ^1H and proton-decoupled ^{31}P and ^{13}C NMR spectra of brain slice extracts were acquired using a Varian INOVA 600 NMR spectrometer (14.1 T) operating at 600.0, 242.79, and 150.82 MHz, respectively. The temperature was regulated at 25ºC for aqueous extracts and 20ºC for lipid extracts. For ^1H NMR, a presaturation pulse sequence was used to minimize the residual water signal. Acquisition parameters included a sweep width of 9611.9 Hz, 2.5-second acquisition time, and 20-second interpulse delay for 256 transients. Data acquisition parameters for ^{31}P aqueous samples included a sweep width of 12121.2 Hz, 1.6-second acquisition time, and 3.6-second interpulse delay for 20,000 transients. ^{13}C lipid acquisition parameters included a sweep

width of 34965 Hz, 1.3-second acquisition time, and 1.9-second interpulse delay for 40,000 transients. ^{31}P lipid data were acquired using a sweep width of 1074.4 Hz, 1.6-second acquisition time, and a 10-second interpulse delay for 768 transients.

The ^{1}H data were processed using exponential multiplication (linebroadening of 0.3 Hz), Fourier transformation, base line corrected using a 5th order polynomial and spline fit, and referenced to TSP set at 0.0 ppm. The ^{31}P aqueous and lipid data used a linebroadening of 1.0 Hz and referenced to phosphocreatine at 0.0 ppm and phosphatidylcholine at -0.84 ppm, respectfully. ^{13}C lipid data used a linebroadening of 0.5 Hz and referenced to MeOH at 49.9 ppm.

Figure 3: Representative ^{1}H aqueous spectrum from rat cortico-hippocampal brain tissue slices.

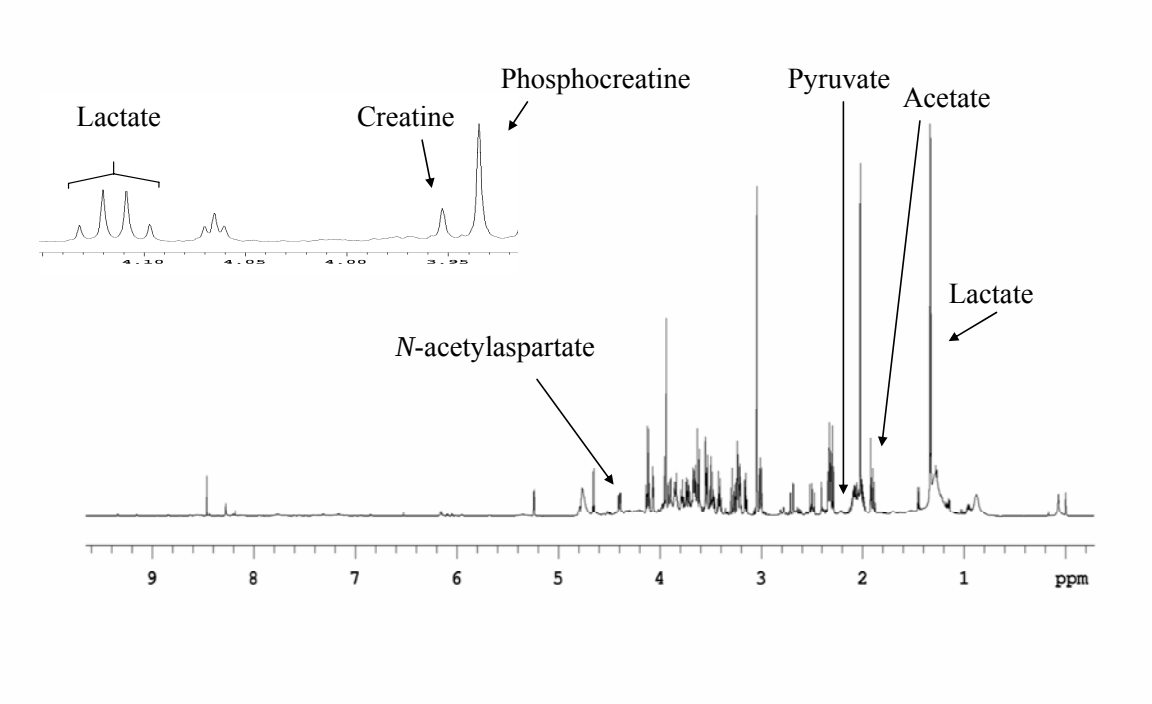


Figure 4: Representative ^{31}P aqueous spectrum from rat cortico-hippocampal brain tissue slices.

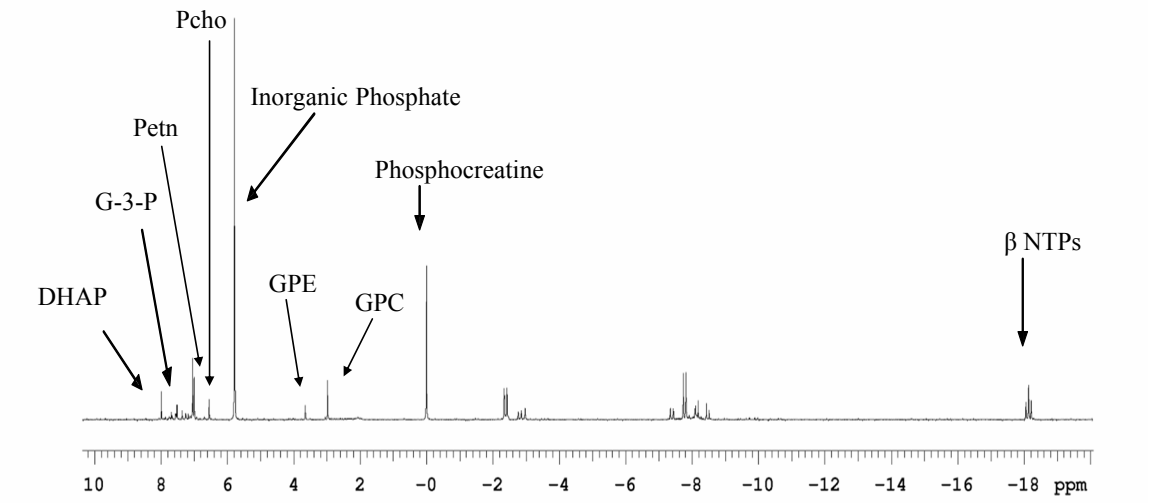


Figure 5: Representative ^{31}P lipid spectrum from rat cortico-hippocampal brain tissue slices.

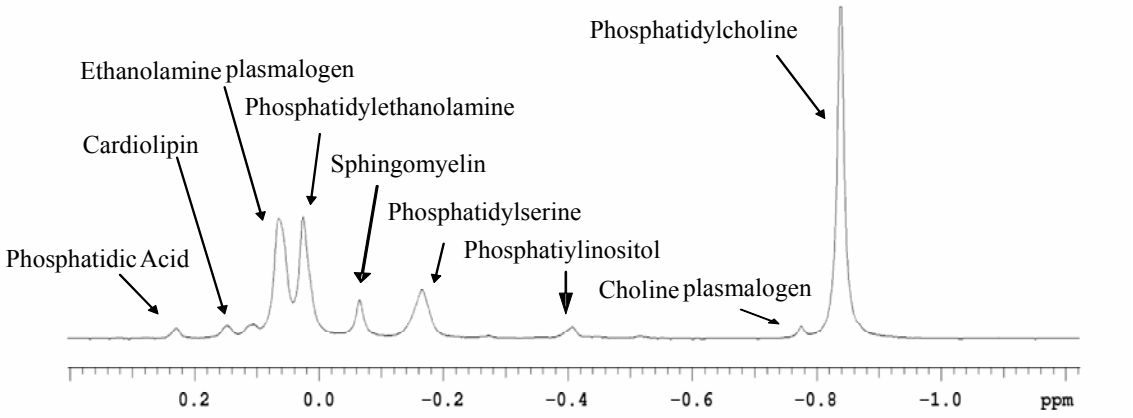
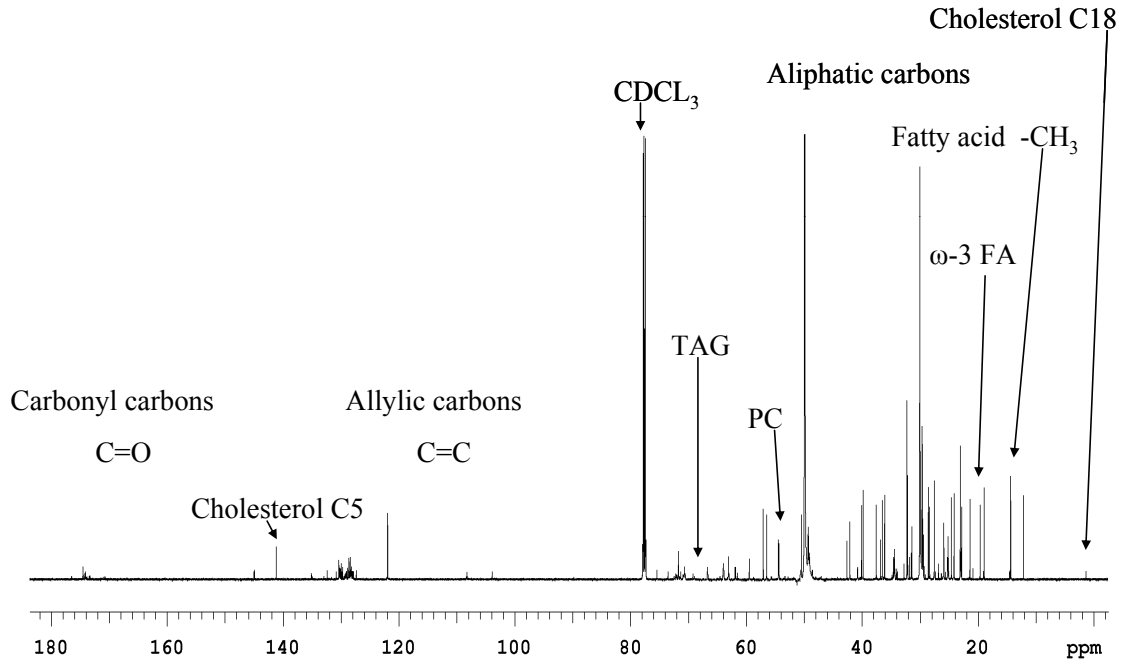


Figure 6: Representative ^{13}C lipid spectrum from rat cortico-hippocampal brain tissue slices.



F. ^{1}H Principle Component Analysis and Linear Discriminant Analysis

Principle Component Analysis (PCA) is a "non-supervised" pattern recognition program that was used to analyze the ^{1}H spectra only. The groups are not identified so it looks for a pattern in the signal intensities of the dataset. The hope is that a group will have the same pattern depending on the treatment received and cluster together to be separated from other groups. PCA reduces a multidimensional dataset into, in this case, a two dimensional dataset by plotting the first two components that are most important in this variance. This program was utilized to determine if groups would cluster according to their exposure to different oxygen concentrations and separate in PCA space due to different metabolite patterns in the datasets.

The spectra were subdivided into 350 regions (bins) and the integrated signal intensities were obtained within each bin. Spectral noise regions were used to determine a threshold level to reduce noise fluctuations that can complicate PCA. The mean and standard deviation (SD) for the noise bin intensities were calculated for each individual spectrum (approximately 100 bins per spectrum), and the threshold value was set at: Mean + 3SD. All bins with values < threshold were then set to zero. The noise regions used to calculate the threshold were then removed along with the regions that contain the residual water signal at 4.80 ppm. The intensity of each integrated signal was normalized to the sum of all metabolite signal intensities within a spectrum. This normalizes the data for different concentrations of metabolites from sample to sample. The signal intensities were then analyzed using PCA to see if treatment groups would separate. If separation does occur, then the data were further analyzed using Linear Discriminate Analysis (LDA), a supervised pattern recognition program. For LDA, the treatment groups are identified and the program determines the importance of each bin in producing a separation in the experimental groups. Each bin is given an LDA weighting factor, which enables the bins to be ranked in order of significance. The data is then plotted with the first LDA projection against the second LDA projection. A query of the program then lists the bins in order of importance. This will give information on which peaks are changing between treatment groups.

Once separation of the data is determined with the sum normalization, the data is then subjected to another form of normalization. Bin normalization occurs when the mean of each bin across all groups is calculated and it is subtracted from the integral within each bin. This is then divided by the standard deviation from the mean for that

bin: (x-mean)/SD. This normalizes the data so that changes in big peaks are weighted the same as small peaks. PCA is performed on this data set. If the groups separate, LDA is then performed. This normalization gives information about the most important bins that cause the most variance in the data across the groups. This then directs our attention to peaks of importance where there could be differences and those peaks can then be integrated to calculate the concentration of each metabolite.

G. Metabolite Quantitative Analysis

NMR data were processed on a Sun Microsystems computer using Varian software (VNMR version 6.1). The dilution factor was calculated according to Equation 1. The saturation factor was calculated according to Equation 2. Proton and phosphorus metabolites and carbon and phospholipid concentrations were determined from each of the aqueous and lipid spectra, according to Equations 3-6, respectively.

DF= Dilution Factor

SF= Saturation Factor calculated for conversion from a saturated spectrum obtained with T_1 saturation and Nuclear Overhouser Effect (NOE) to a fully relaxed spectrum obtained without NOE.

M= Metabolite of interest

I= Intensity of peak

FR= Fully relaxed spectrum

Sat= Saturated spectrum

Std= Standard

Equation 1:

$$DF = \frac{\text{Volume in sample vial (mL)}}{\text{Volume drawn up from vial}}$$

Equation 2:

$$SF = \frac{\left(\frac{I_M}{I_{Std}}\right) FR}{\left(\frac{I_M}{I_{Std}}\right) Sat}$$

Equation 3:

$$[M]^{1H}_{AQS} = \frac{\left(\frac{(I_M/\#\text{ of equivalent }^1H)}{I_{TSP}/9} \bullet [Std(mM)]\right) \bullet DF \bullet \text{Total Volume in NMR tube (mL)}}{\text{Brain slice weight (g)}}$$

Equation 4:

$$[M]^{31P}_{AQS} = \frac{SF \bullet \left(\frac{I_M}{I_{MDPA}} \bullet [Std(mM)]\right) \bullet DF \bullet \text{Total Volume in NMR tube (mL)}}{\text{Brain slice weight (g)}}$$

Equation 5:

$$[M]^{13C}_{Lpd} = SF \bullet \frac{\left(\frac{I_M}{I_{CDCL3}} \bullet [Std(mM)]\right) \bullet DF \bullet \text{Total Volume in NMR tube (mL)}}{\text{Brain slice weight (g)}}$$

Equation 6:

$$[M]^{31P}_{Lpd} = \frac{\left(\frac{I_M}{I_{PC}} \bullet [Std(mM)]\right) \bullet DF \bullet \text{Total Volume in NMR tube (mL)}}{\text{Brain slice weight (g)}}$$

H. Statistical Analysis

Once the concentrations of each metabolite were calculated, statistical analysis was performed using JMP version 5.1.2. ANOVA and Tukey HSD with a p value of 0.05 set for statistical significance.

Chapter IV

Results

A. Correction Factor for Tissue Sample Weight

The weight of tissue slices after exposure to hyperbaric oxygen (4.50 ATA) for 60 minutes are 23% lower in comparison to tissue slices exposed to either 0.40 ATA or 0.95 ATA O_2 at ambient pressure for the same time period (Table I). Whether this is due to an effect of oxygen concentration or pressure is unclear. However, an experiment conducted at 0.95 ATA O_2 and ambient pressure showed that tissue slices exposed for 5 minutes yielded weights that were 22% lower than tissues exposed for 60 minutes. Therefore, it appears that over time the tissue slices may retain more water. Since the 0.40 ATA and 0.95 ATA O_2 groups measured at 60 minutes yield similar weights, this suggests that oxygen concentration is not a factor (at least in this oxygen range). Therefore, we hypothesize that water is not retained in the tissue slices of the 4.50 ATA O_2 group due to pressurization.

To test this hypothesis, tissue slices were incubated in 0.95 ATA O_2 and pressurized using helium gas instead of oxygen. Briefly, tissue slices (approximately 12 slices per rat) were prepared and allowed a 1-hour recovery period as described previously. The slices were exposed to a gas mixture at 4.50 ATA containing 76.5% He, 22.3% O_2 and 1.2% CO_2 for 60 minutes (full compression achieved in < 5 min). This helium mixture allowed for the slices to be exposed to the equivalent of 95% O_2 and 5%

CO_2 for comparison with previous experiments. Following decompression (<5 min) the slices were rinsed with saline in a strainer, blotted dry, and frozen in liquid N_2 (< 2 minutes). Slices from two animals were pooled (~24 slices) to provide a single tissue sample, consistent with our previous experimental procedures. The slices were powdered with a mortar and pestle under liquid N_2 and then transferred into a homogenizer tube to determine the weight of each tissue sample. Weights are expressed as mean ± SD (mg/slice).

TABLE I. Tissues slice weights for each experimental group (mg per slice, Mean ± SD). * Denotes significant difference from 0.40 ATA (ANOVA and Tukey HSD, $p \leq 0.05$).

Weights as a Function of O_2 Concentration			**Weights as a Function of Time**		**Weights as a Function of Pressurized Gas**	
0.40 ATA 60 min	**0.95 ATA 60 min**	**4.50 ATA 60 min**	**0.95 ATA 60 min**	**0.95 ATA 5 min**	**4.50 ATA O_2 60 min**	**4.50 ATA He 60 min**
30.4±5.7 (n=6)	29.8±3.3 (n=6)	23.5±2.3 * (n=6)	29.8±3.3 (n=6)	23.3±3.0 (n=4)	23.5±2.3 (n=6)	25.6±3.0 (n=4)
Calculated Mean Weight per Slice (mg)						
0.95 ATA O_2 5 min, 4.50 ATA O_2 60 min, 4.50 ATA He 60 min						
24.03±2.7 (n=14)						

Table I shows tissue slice weights for each experimental group (mg per slice, Mean±SD) as a function of oxygen, time, and pressurized gas. Comparison by unpaired t-test of the samples that were pressurized, HBO group and the hyperbaric helium group (HBHe), showed no differences between the weights. A comparison of all the groups that had lower weights, 0.95 ATA O_2 at 5 minutes, 4.50 ATA O_2, and 4.50 ATA He, showed no differences between groups (ANOVA, $p \leq 0.05$). These lower weight groups were then combined together and compared to the combination of the two groups with greater weight per slice at ambient pressure, namely the 0.40 ATA and 0.95 ATA O_2 at

60 minutes groups. The weights of the ambient pressure group were significantly greater than the pressurized group (t-test, $p \leq 0.05$). It appears that over time the tissue slices swell with water, but pressure at 4.50 ATA prevents this swelling independent of whether oxygen or helium was used for pressurization. Therefore, this leads to the conclusion that the lower tissue weight is an effect of pressure, but not of oxygen.

This was then enough evidence to conclude that a correction factor needed to be calculated to adjust for the extra weight of water. The mean of the weight per slice of the 4.50 ATA O_2, 4.50 ATA He, and 0.95 ATA O_2 at 5 minutes groups was calculated as 24.03 mg/slice with a percent standard deviation of 11%. The number of slices per sample was then multiplied by this mean to give the correct amount of brain tissue in grams of that sample. This corrected brain weight was then used to calculate the amount of metabolite per gram of tissue for all experimental groups.

B. Principal Component Analyses and Discriminate Analyses

A PCA scores plot (Figure 7) for slice aqueous metabolites measured by ^{1}H NMR shows a separation between experimental groups (A), all O_2 levels at 60 min (B), and 0.95 ATA O_2 at 5 and 60 min (C).

Figure 7A: PCA scores plot from ^{1}H aqueous spectra. Bright blue lines= 0.40 ATA, green lines= 0.95 ATA at 60 min, red lines= 4.50 ATA, dark blue lines= 0.95 ATA at 5 min

:

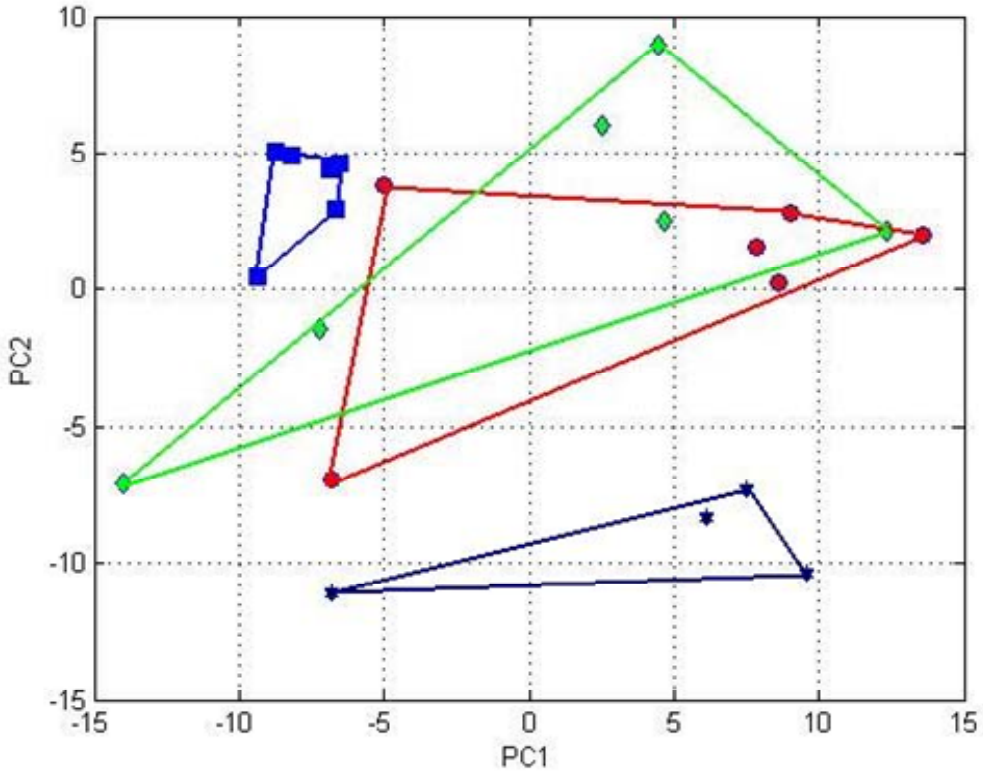


Figure 7B: PCA scores plot from ^{1}H aqueous spectra. Bright blue lines= 0.40 ATA, green lines= 0.95 ATA at 60 min, red lines= 4.50 ATA

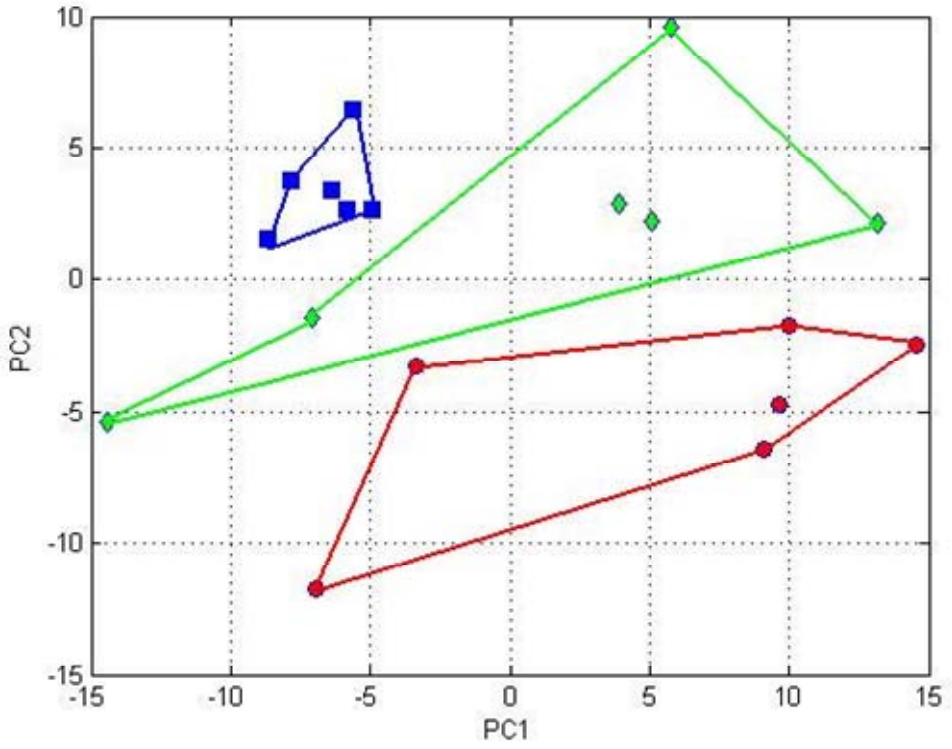
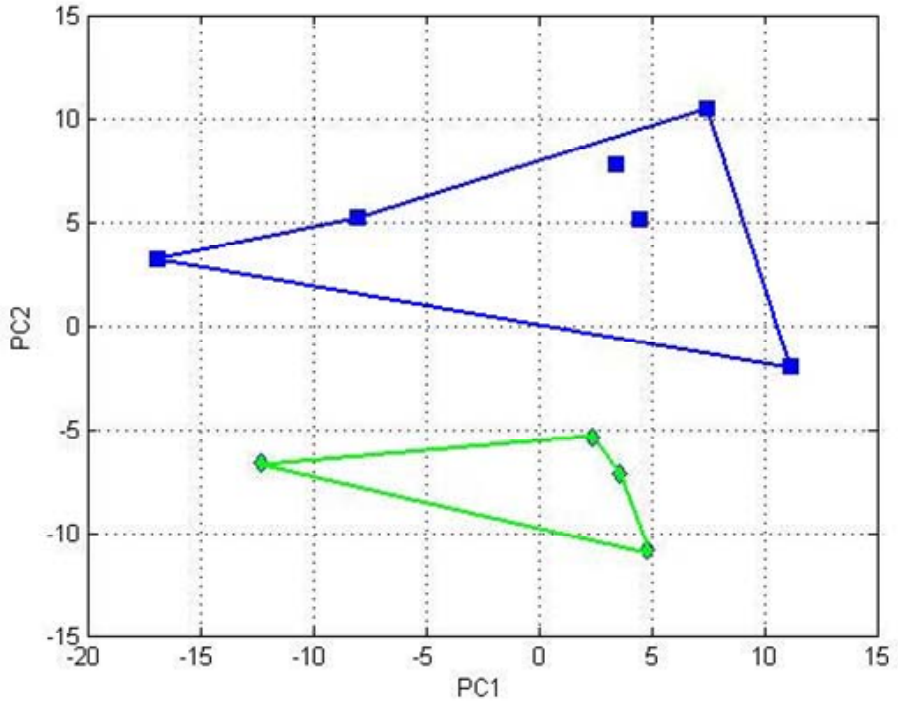


Figure 7C: PCA scores plot from ^{1}H aqueous spectra. Bright blue lines= 0.95 ATA at 60 min green lines= 0.95 ATA at 5 min



These graphs show a plot of principal component 1 (PC1) versus principle component 2 (PC2) which are the two most important components that show variance in the dataset. These components are plotted against each other and show a separation of the groups according to the oxygen treatment that was received.

Further analysis using LDA (figure 8) shows separation between all experimental groups (A), all groups at 60 minutes (B), and 0.95 ATA O_2 at 5 and 60 minutes(C).

Figure 8A: LDA projection plot from ^{1}H aqueous spectra. Red lines = 0.40 ATA, blue lines = 0.95 ATA at 60 min, green lines = 4.50 ATA, aqua lines= 0.95 ATA at 5 min

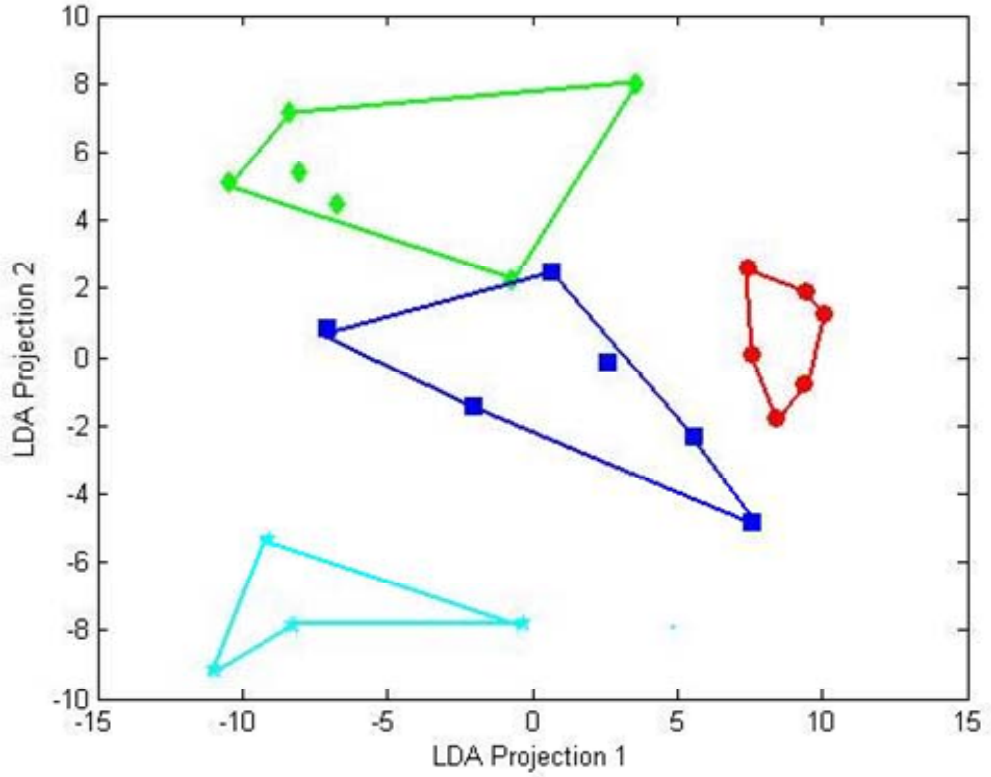


Figure 8B: LDA projection plot from ^{1}H aqueous spectra. Red lines = 0.40 ATA, blue lines = 0.95 ATA at 60 min, green lines = 4.50 ATA

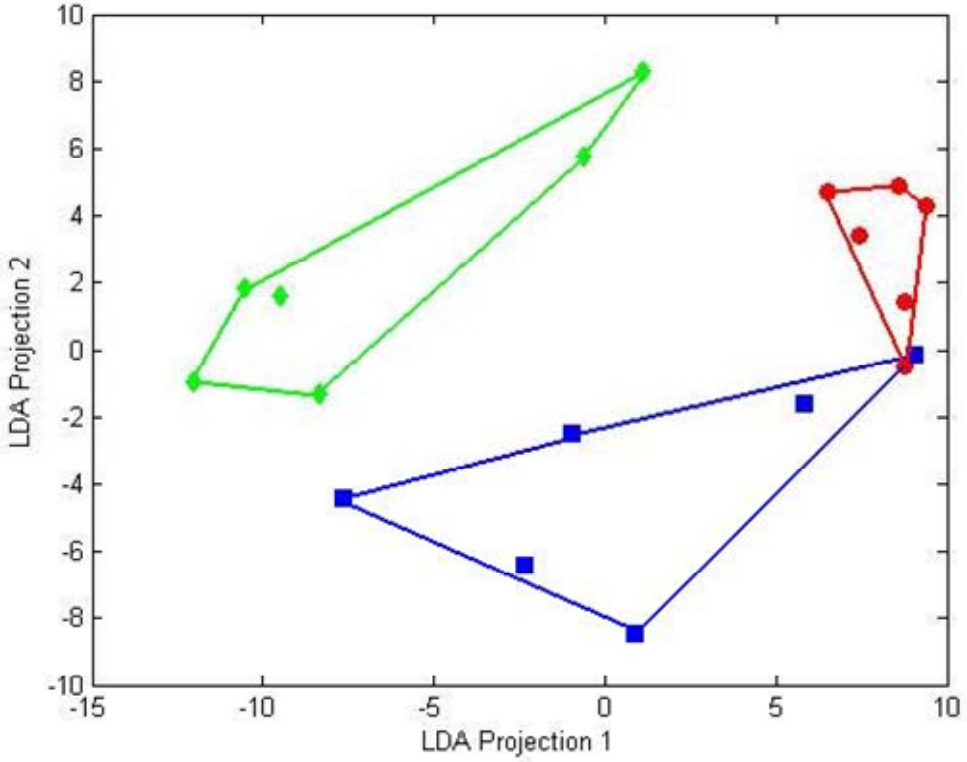
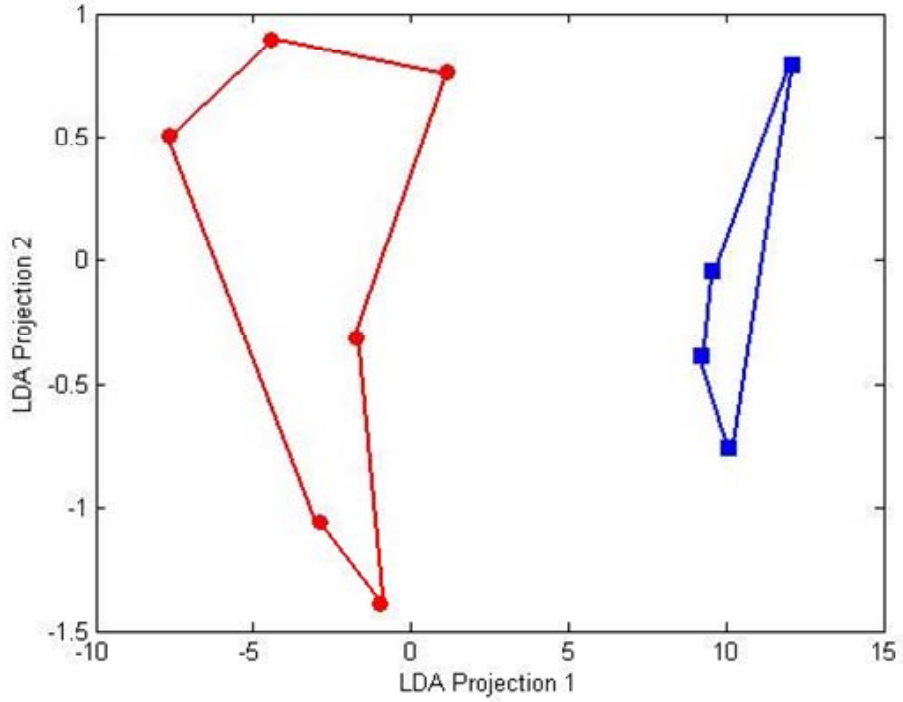


Figure 8C: LDA projection plot from ^{1}H aqueous spectra. Red lines = 0.95 ATA at 60 min, blue lines= 0.95 ATA at 5 min



These graphs show a plot of LDA projection 1 versus LDA projection 2. Since the program knows the identification of the groups, it tries to separate according to differing profiles between the groups. These graphs show that there was separation between the experimental groups. A query of the program gave a list of LDA weighting factors (coefficients) and identified the spectral regions (bins or PPM values) that cause the separation (Table II). This list was then used as a guide to look at different metabolites within the spectra.

TABLE II. Highest ranked ^{1}H aqueous LDA weighting factors, PPMs, and identified metabolites.

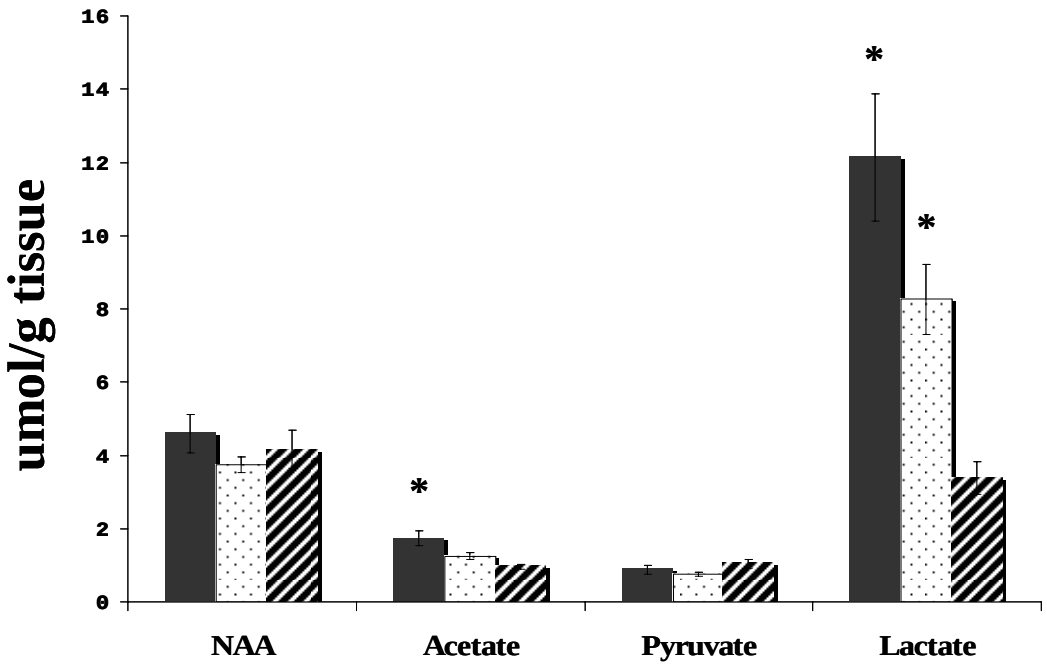
^{1}H Aqueous Linear Discriminate Analysis				
Weighting Factor	**PPM**	**Metabolite**	**Corresponding ^{1}H**	**Multiplicity**
-0.1566	1.32	Lactate	$^{3}CH_3$	Doublet
0.1563	3.96	Creatine and Phosphocreatine (Cr and PCr)	$^{2}CH_2$	Singlet
-0.1502	4.12	Lactate	^{2}CH	Quartet
0.1186	2.36	Pyruvate	$^{3}CH_3$	Singlet
0.1151	4.40	N-acetylaspartate (NAA)	^{2}CH	Doublet of doublet
-0.1134	1.88	Acetate	$^{2}CH_3$	Singlet

C. Metabolite Analyses from ^{1}H Aqueous Spectra

Figure 9 is a graph of some of the quantified (μmol/g tissue, Mean±SE) salient metabolites identified from LDA. N-acetylaspartate (NAA) shows no differences across all 60 minute time point groups. Acetate was elevated in 0.40 ATA O_2 group by 80% compared to the 4.50 ATA O_2 group. Pyruvate showed no differences between 60 minute

time point groups, but for lactate the 4.50 ATA O_2 group was significantly lower compared to both 0.95 ATA O_2 at 60 minutes (60%) and 0.40 ATA O_2 (73%).

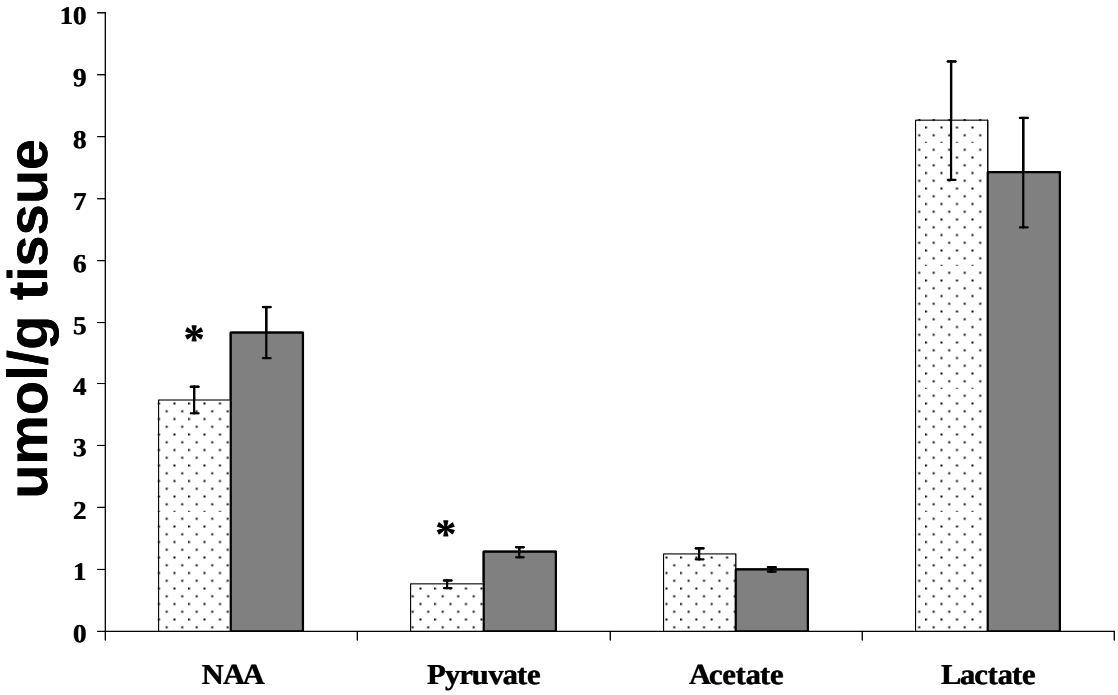
Figure 9: Quantified ^{1}H aqueous metabolites (umol/g tissue,Mean±SE). Filled black bars= 0.40 ATA O_2, white polka dot bars=0.95 ATA O_2 at 60 minutes, black hatched bars=4.50 ATA O_2



* denotes significant difference from 4.50 ATA O_2 (ANOVA, Tukey HSD $p \leq .05$).

Figure 10 shows a comparison of 0.95 ATA O_2 groups at different time points, 60 minutes and 5 minutes. NAA and pyruvate were significantly lower in the 0.95 ATA O_2 at 60 minutes group compared to the 0.95 ATA O_2 at 5 minutes group. No differences were found for acetate or lactate between these groups.

Figure 10: Quantified ^{1}H aqueous metabolites (umol/g tissue, Mean±SE)
White polka dot bars=0.95 ATA O_2 at 60 minutes, filled white bars=0.95 ATA O_2 at 5 minutes

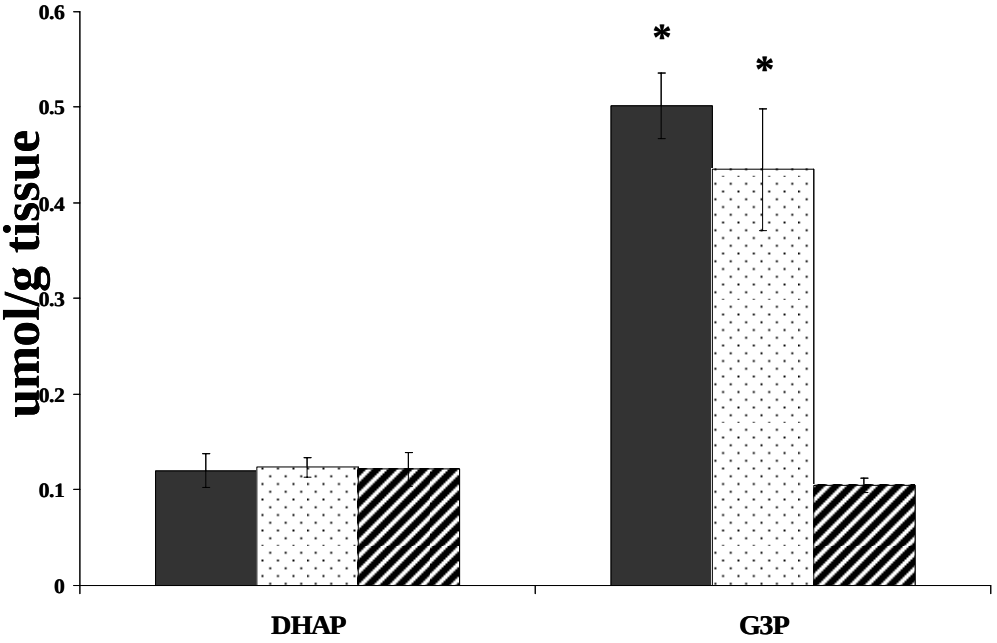


* denotes significant difference from 0.95 ATA O_2 at 5 minutes (t-test, $p \leq .05$).

D. Metabolite Analyses from ^{31}P Aqueous Spectra

Figure 11 shows phosphorus metabolites that can be identified from the ^{31}P spectra. Dihydroxyacetone phosphate (DHAP) showed no differences between groups. Glycerol-3-phosphate (G3P) showed that 0.40 ATA O_2 group and 0.95 ATA O_2 group were not different, but that they were both about a 5-fold increase over the 4.50 ATA O_2 group.

Figure 11: Quantified ^{31}P aqueous metabolites (umol/g tissue,Mean±SE). Filled black bars= 0.40 ATA O_2, white polka dot bars=0.95 ATA O_2 at 60 minutes, black hatched bars=4.50 ATA O_2

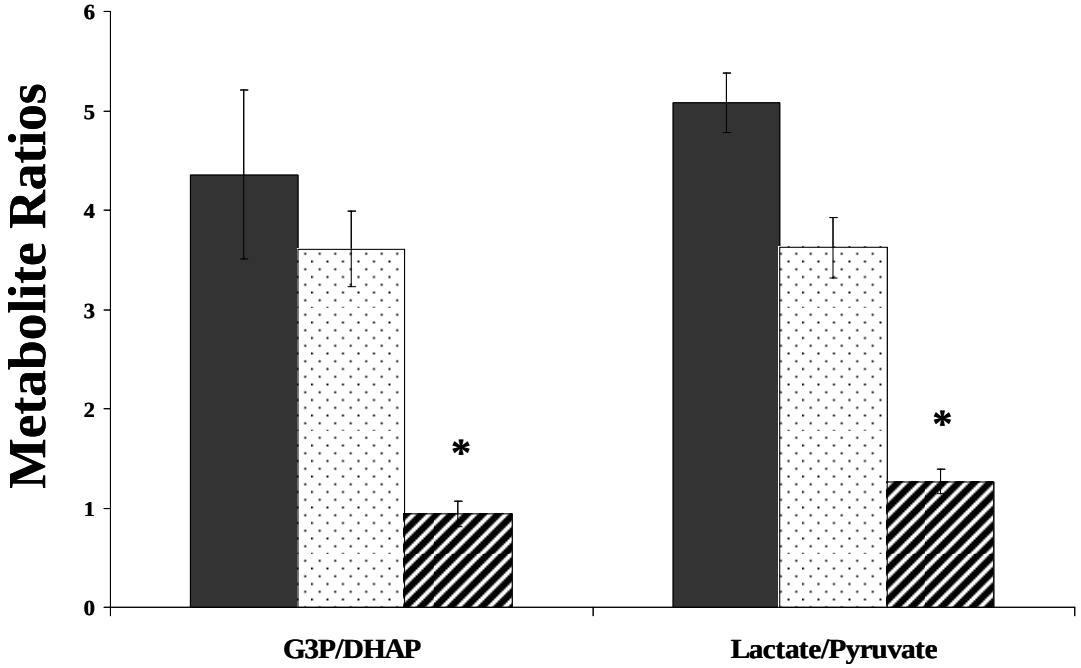


* denotes significant difference from 4.50 ATA O_2 (ANOVA, Tukey HSD $p \leq .05$).

E. Metabolite Ratios

Figure 12 shows metabolite ratios of G3P/DHAP and lactate/pyruvate. The 4.50 ATA O_2 group is significantly lower than both the 0.40 ATA and 0.95 ATA O_2 at 60 minute groups (78%) with respect to G3P/DHAP ratio. With respect to the lactate/pyruvate ratio, the 4.50 ATA O_2 group is significantly lower than the 0.40 ATA (71%) and 0.95 ATA O_2 groups (65%).

Figure 12: Metabolite ratios from ^{31}P and ^{1}H aqueous spectra. Filled black bars= 0.40 ATA O_2, white polka dot bars=0.95 ATA O_2 at 60 minutes, black hatched bars=4.50 ATA O_2



* denotes significant difference from 0.40 ATA O_2 and 0.95 ATA O_2 (ANOVA, Tukey HSD $p \leq .05$).

Figure 13 illustrates a correlation between O_2 concentration and the G3P/DHAP and the lactate/pyruvate ratios. Both of these metabolite ratios decrease with increasing oxygen concentration, and the data fit a linear correlation fairly well (r^2=0.95).

Figure 13: Ratios of G3P/DHAP and Lactate/Pyruvate plotted per oxygen concentration. 0.40 ATA 0.95 ATA, and 4.50 ATA O_2

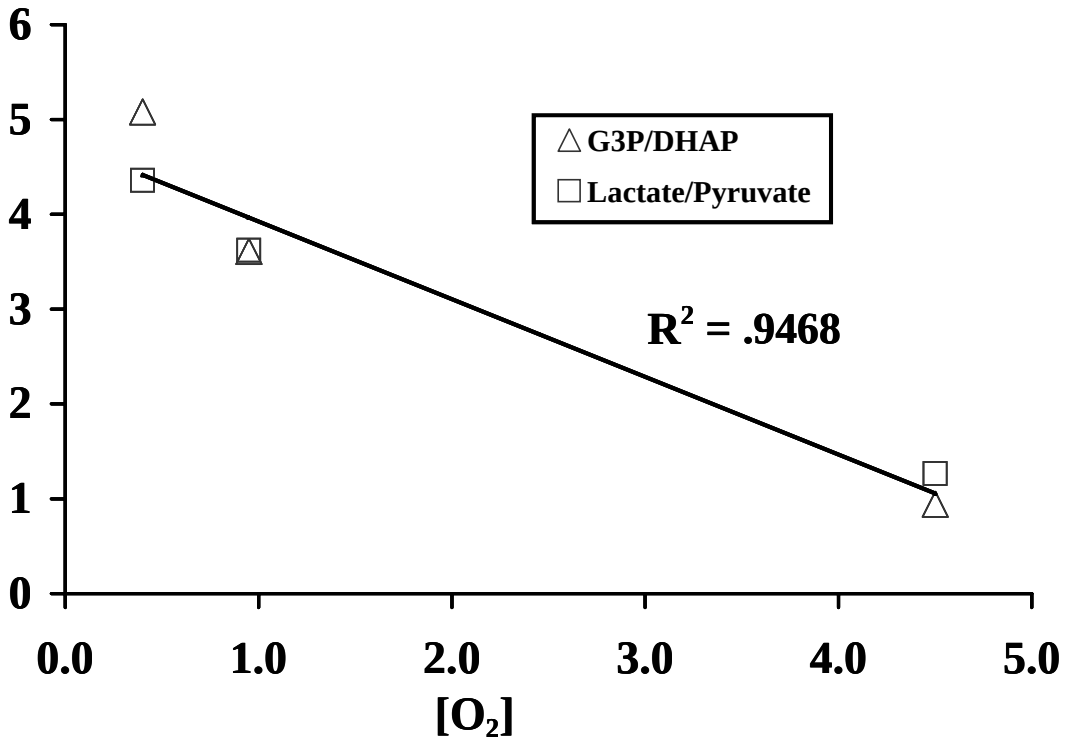
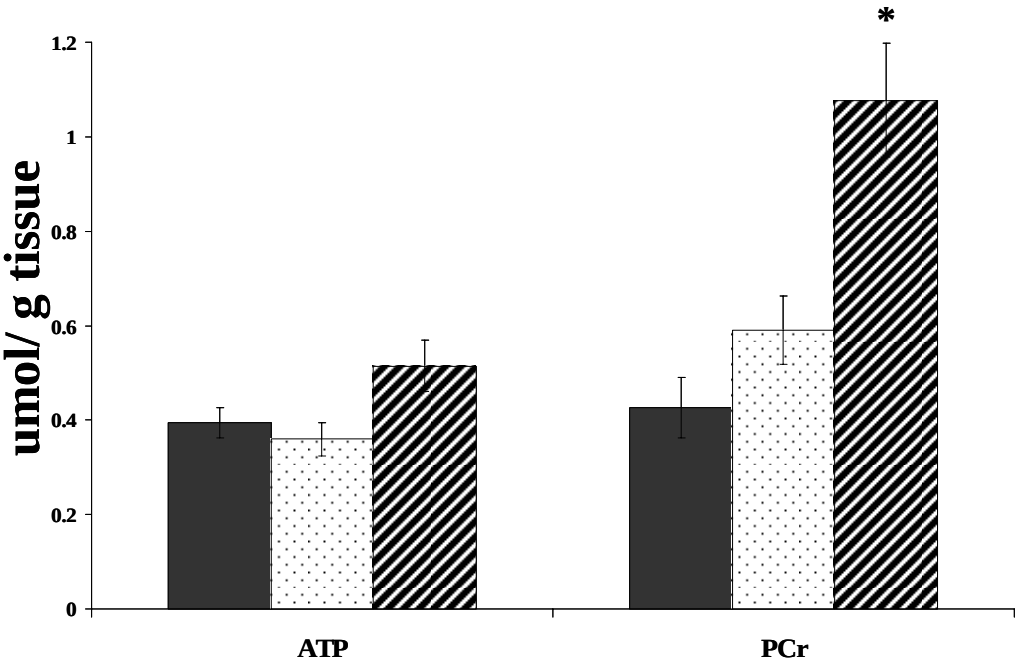


Figure 14 shows high energy phosphate metabolites from the ^{31}P spectra. The Adenosine triphosphate (ATP) showed no differences across groups, but the 4.50 ATA O_2 phosphocreatine (PCr) was greater compared to both 0.40 ATA (153%) and 0.95 ATA O_2 (82%), although there were no differences in inorganic phosphate (Pi, Figure 15).

Figure 14: Quantified ^{31}P aqueous metabolites (umol/g tissue,Mean±SE). Filled black bars= 0.40 ATA O_2, white polka dot bars=0.95 ATA O_2 at 60 minutes, black hatched bars=4.50 ATA O_2



* denotes significant difference from 0.40 ATA O_2 and 0.95 ATA O_2 (ANOVA, Tukey HSD $p \leq .05$)

Figure 15: Quantified ^{31}P aqueous metabolites (umol/g tissue, Mean±SE). Filled black bars= 0.40 ATA O_2, white polka dot bars=0.95 ATA O_2 at 60 minutes, black hatched bars=4.50 ATA O_2

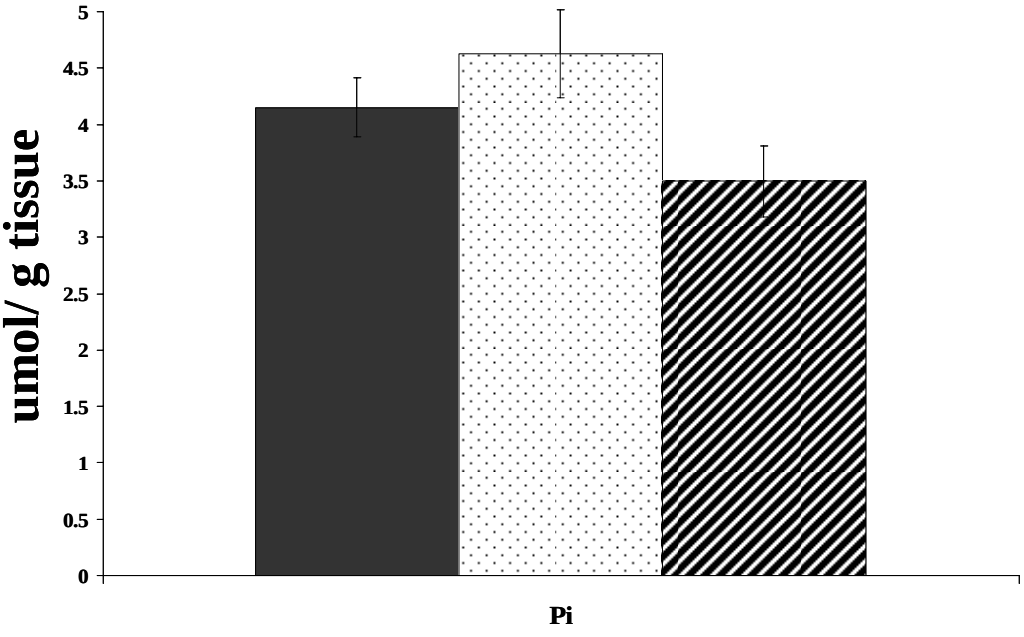
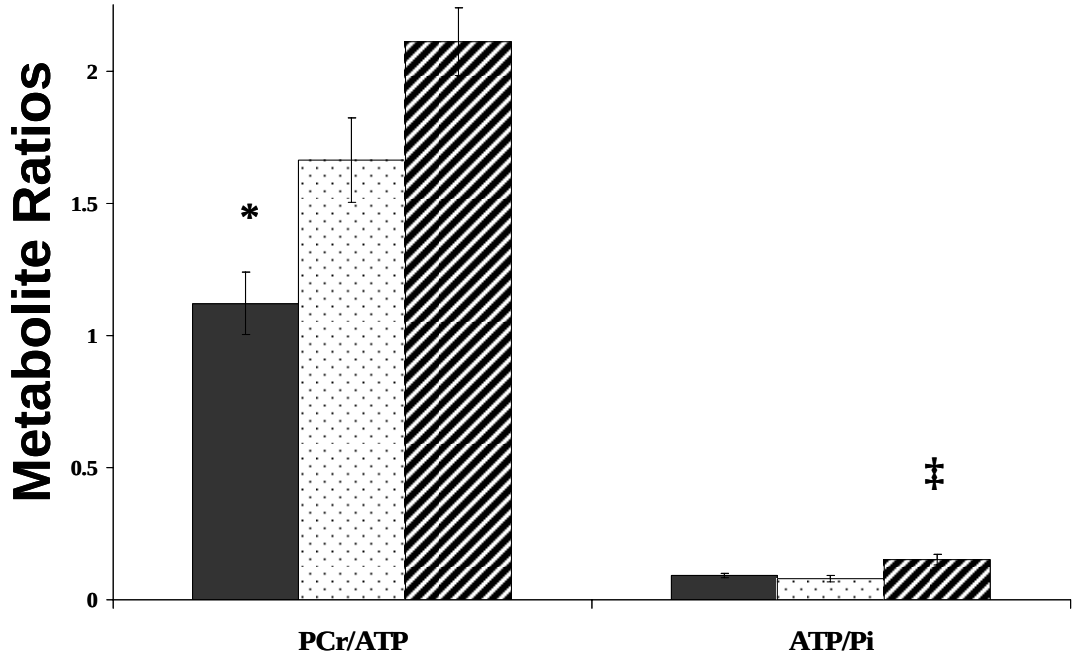


Figure 16 shows high energy phosphate ratios from the phosphorus aqueous spectra. The 0.40 ATA O_2 group is lower than both the 0.95 ATA O_2 and 4.50 ATA O_2 groups for PCr/ATP. The ATP/Pi ratio for the 4.50 ATA O_2 group is greater than both the 0.40 ATA and 0.95 ATA O_2 groups.

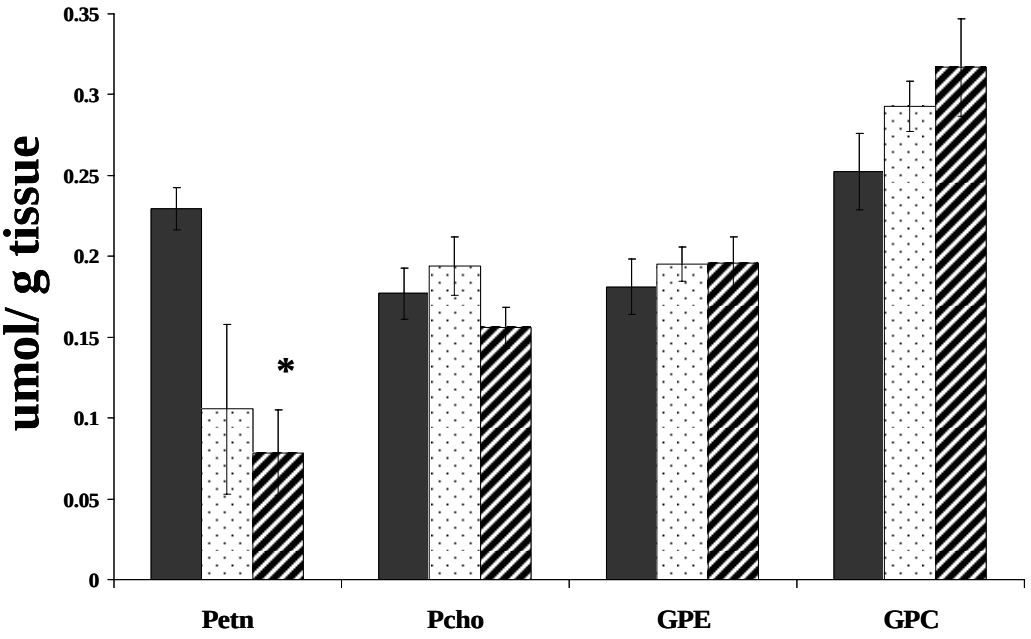
Figure 16: Metabolite ratios from ^{31}P aqueous spectra. Filled black bars= 0.40 ATA O_2, white polka dot bars=0.95 ATA O_2 at 60 minutes, black hatched bars=4.50 ATA O_2



*denotes significant difference from 0.95 ATA O_2 and 4.50 ATA O_2 (ANOVA, Tukey HSD $p \leq .05$)
‡denotes significant difference from 0.40 ATA O_2 and 0.95 ATA O_2 (ANOVA, Tukey HSD $p \leq .05$)

Figure 17 shows phosphorous metabolites involved in phospholipid synthesis and degradation pathways. The 4.50 ATA O_2 group phosphoethanolamine (Petn) was 66% lower compared to 0.40 ATA O_2 group. There were no differences seen between groups with phosphocholine (Pcho), glycerophosphoethanolamine (GPE), or glycerophosphocholine (GPC).

Figure 17: Quantified ^{31}P aqueous metabolites (umol/g tissue,Mean±SE). Filled black bars= 0.40 ATA O_2, white polka dot bars=0.95 ATA O_2 at 60 minutes, black hatched bars=4.50 ATA O_2

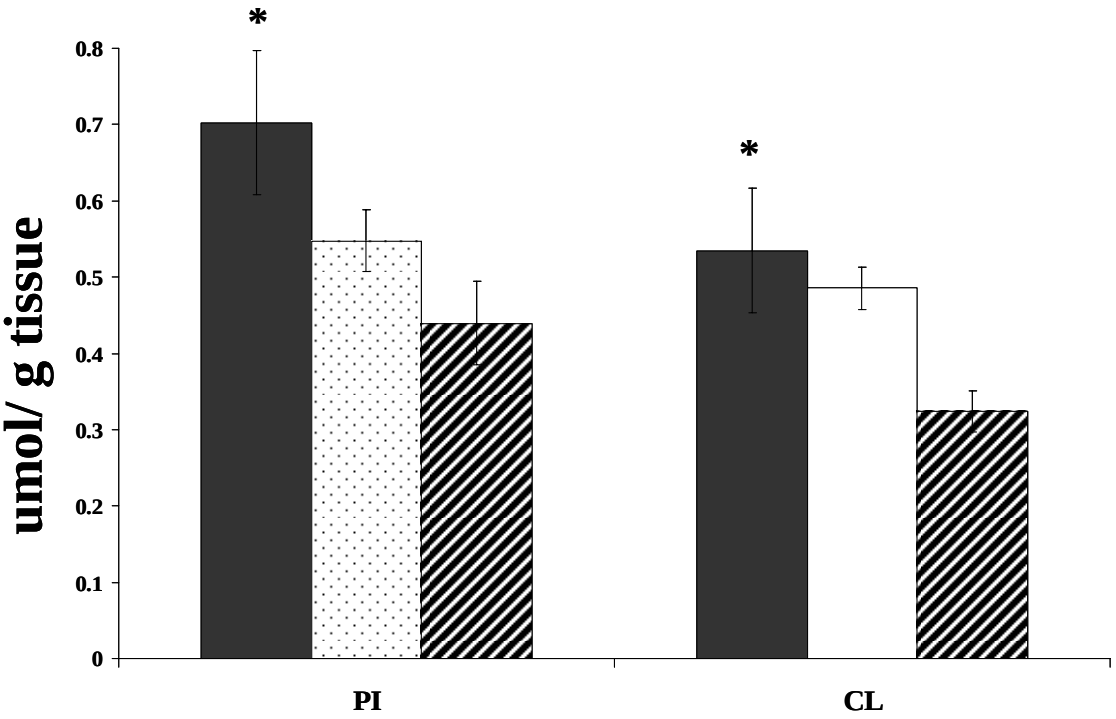


* denotes significant difference from 0.40 ATA O_2 (ANOVA, Tukey HSD $p \leq .05$).

F. Metabolite Analyses from ^{31}P Lipid Spectra

Figure 18 shows the quantification of phospholipids from the ^{31}P lipid spectra. The 0.40 ATA O_2 phosphatidylinositol (PI) is 60% greater than the 4.50 ATA O_2. Cardiolipin (CL) was also greater by 65% in 0.40 ATA O_2 compared to 4.50 ATA O_2. There were no significant differences in Phosphatidylethanolamine, Sphingomyelin, Phosphatidylserine, Choline plasmalogen, or Phosphatidylcholine. There were no significant differences in Phosphoatidylethanolamine plasmalogen or phosphatidic acid, but they did show a trend to decrease with increasing oxygen concentration (Table III).

Figure 18: Quantified ^{31}P lipids (umol/g tissue,Mean±SE). Filled black bars= 0.40 ATA O_2, white polka dot bars=0.95 ATA O_2 at 60 minutes, black hatched bars=4.50 ATA O_2



* denotes significant difference from 4.50 ATA O_2 (ANOVA, Tukey HSD $p \leq .05$).

TABLE III. Quantified ^{31}P phospholipids (μmol/ g tissue, Mean ± SE).

Phosphorus Lipid Quantitation			
	0.40 ATA (n=5)	**0.95 ATA 60 min (n=6)**	**4.50 ATA (n=6)**
Phosphatidylethanolamine plasmalogen (PE pls)	7.23 ± 0.76	6.40 ± 0.35	5.24 ± 0.45
Phosphatidylinositol (PI)	0.70 ± 0.09 *	0.55 ± 0.04	0.44 ± 0.06
Cardiolipin (CL)	0.53 ± 0.08 *	0.48 ± 0.03	0.32 ± 0.03
Phosphatidic Acid (PA)	0.35 ± 0.05	0.29 ± 0.02	0.22 ± 0.02

* denotes significant difference from 4.50 ATA O_2 (ANOVA, Tukey HSD $p \leq .05$)

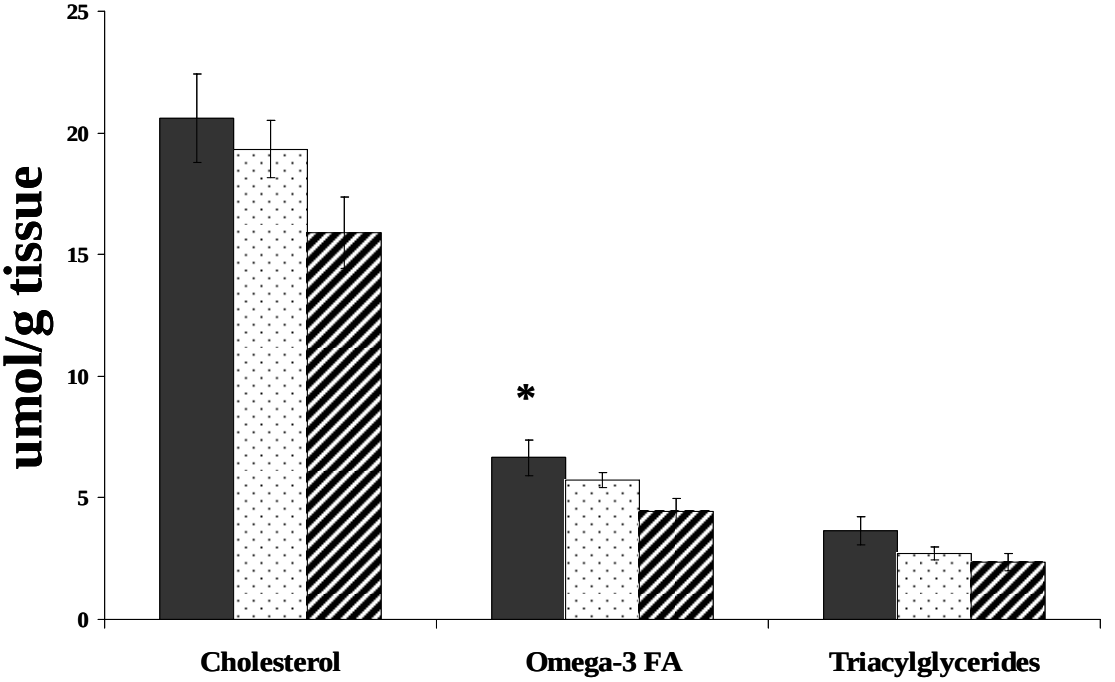
G. Metabolite Analyses from ^{13}C Lipid Spectra

TABLE IV. Carbon lipid peaks and respective PPM.

^{13}Carbon Lipid Metabolites	
PPM	**Metabolite**
141.3	Cholesterol carbon 5
12.3	Cholesterol carbon 18
54.6	Phosphatidylcholine
21.0	Omega-3 Fatty Acids
69.1	Triacylglycerides

Figure 19 shows the quantification of carbon lipids from the ^{13}C lipid spectra. There were no differences between groups at 60 minutes for cholesterol and triacylglycerides, but both trend toward a decrease with increasing oxygen. Omega-3 fatty acids show a significant decrease from 0.40 ATA O_2 group to 4.50 ATA O_2 group with the same decreasing trend with increasing oxygen.

Figure 19: Quantified ^{13}C lipids (umol/g tissue,Mean±SE). Filled black bars=0.40 ATA O_2, white polka dot bars=0.95 ATA O_2 at 60 minutes, black hatched bars=4.50 ATA O_2



* denotes significant difference from 4.50 ATA O_2 (ANOVA, Tukey HSD $p \leq .05$).

H. Time Dependence of Metabolite Ratios

Table V shows a comparison of metabolite ratios for 0.95 ATA O_2 at 60 minutes vs. 5 minutes. Significant differences were found for Lactate/Pyruvate, G3P/DHAP, Petn/PE, Petn/PE Pls, and Petn/GPE.

TABLE V. Metabolite Ratios (Mean ± SE).

Metabolite Ratios for 0.95 ATA O_2 60 minutes vs. 5 minutes		
	0.95 ATA 60 min (n=6)	**0.95 ATA 5 min (n=4)**
Lactate/Pyruvate	3.62 ± 0.30 *	1.88 ± 0.15
PCr/ATP	1.66 ± 0.16	2.08 ± 0.20
ATP/Pi	0.08 ± 0.01	0.06 ± 0.01
G3P/DHAP	3.61 ± 0.38 *	1.30 ± 0.21
Petn/PE	8.50 ± 1.50 *	20.04 ± 0.34
Petn/PE Pls	6.34 ± 1.04 *	14.56 ± 0.29
Petn/GPE	0.12 ± 0.02 *	0.26 ± 0.01

* denotes significant difference from 0.95 ATA O_2 at 5 minutes (t-test, $p \leq .05$)

Chapter V

Discussion

A. PCA and LDA Analysis

Separation between experimental groups using PCA scores plots for ^{1}H NMR suggests that the tissue metabolite profile changes are induced by O_2 (Figure 7). This was further examined by using LDA to identify salient metabolites that caused the separation (Figure 8). The metabolite list generated was further examined by quantifying metabolites from the spectra and comparing each group (Table II).

B. Neuronal Cell Viability

NMR measurements of chemical extracts provide a metabolite profile from the entire tissue slice and cannot discern glial from neuronal cell types. However, N-acetylaspartate (NAA) is a marker of neuronal cell viability and can be quantified. This will show whether the neuron population, which is sensitive to oxygen concentration, is dying. There were no differences in NAA, which suggests that these oxygen concentrations did not adversely affect the neurons (Figure 9). But, overall tissue metabolism showed differences in response to O_2 concentrations.

C. Oxygen Effects on Energy Metabolism

By examining the ^{1}H spectra, insight can be gained into the function of glycolysis and the TCA cycle (Figure 9). Acetate and Lactate were both elevated in the 0.40 ATA

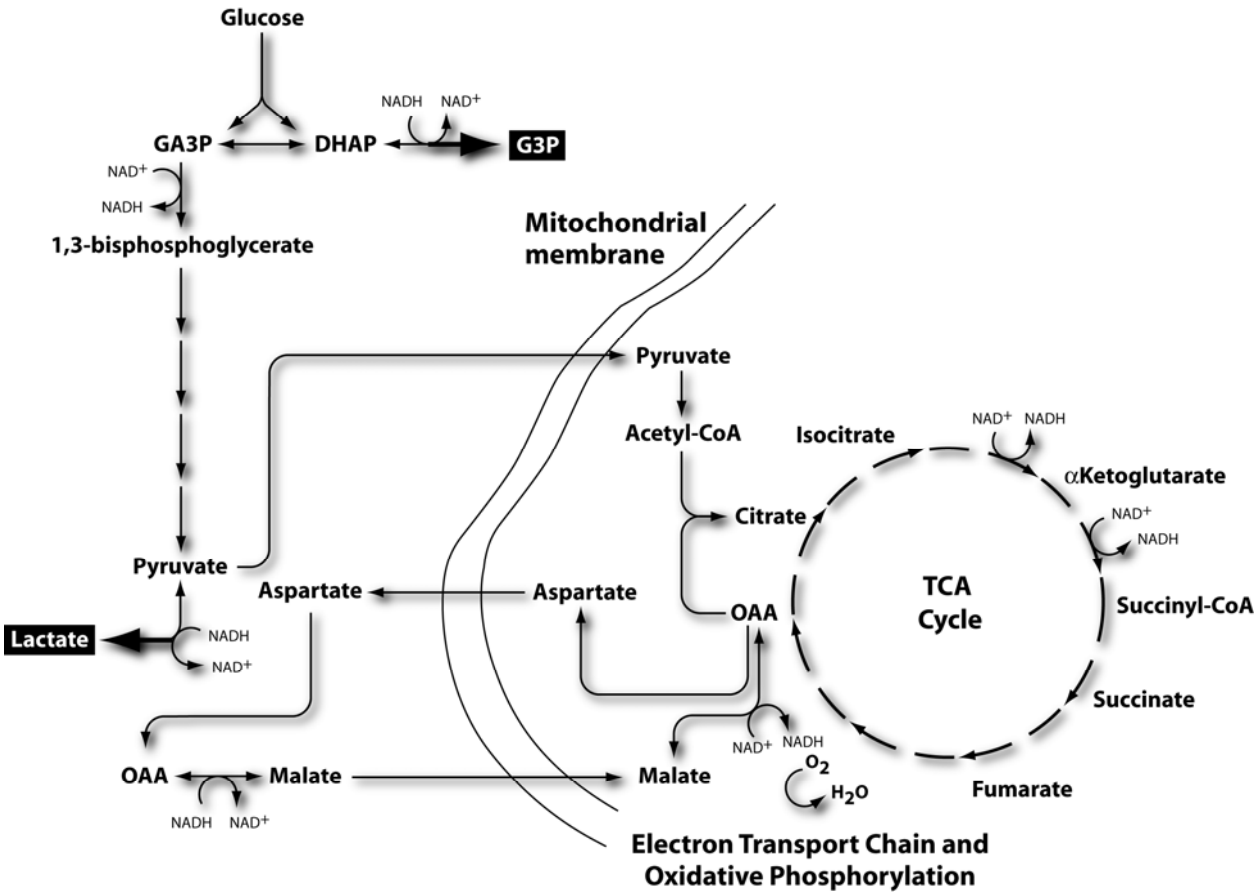
O_2 group. This may be indicative of a hypoxic environment and the cells are using anaerobic glycolysis to generate ATP through lactate and the acetate is elevated because it is not used to make acetyl-CoA for input into the TCA cycle. Lactate is also lower in 4.50 ATA O_2 where oxidative phosphorylation is running well because there is an abundance of oxygen. There were no differences in pyruvate between all groups. This could be because it is being utilized in the 4.50 ATA O_2 group in the TCA cycle and being converted to lactate in 0.40 ATA O_2 group.

The increase in NAA and pyruvate in the 0.95 ATA O_2 at 60 minutes compared to the 0.95 ATA O_2 at 5 minutes (Figure 10) may be the result of the tissue damage caused by slicing. During the recovery and treatment period, the membranes of the cells repair themselves so there is increased metabolism and use of pyruvate to generate ATP. The stores may be replenished during the 60 minute treatment period resulting in more pyruvate at the 60 minute time point compared to the 5 minute time point.

Examining the ^{31}P aqueous spectra gives insight into the energy metabolism of the slices and supports the previous conclusions about oxidative phosphorylation. ATP and PCr both are elevated in 4.50 ATA O_2 group and Pi trends to being lower, but is not significant (Figure 14 and Figure 15). This suggests that the tissue slices have a good energy status. The PCr/ATP ratio (Figure 16) is the same as reported *in vivo* in humans at 2.1 ± 0.13 [41-43] This strengthens the conclusion that oxidative phosphorylation is running well in 4.50 ATA O_2 group, which is hyperoxic, and that 0.40 ATA O_2 may be becoming hypoxic. In this same spectra, peaks for DHAP and G3P can be examined that will give insight into the cytosolic redox potential of the cells (Figure 11). There were no changes in DHAP, but G3P was lower in 4.50 ATA O_2 group than the other 60 minute

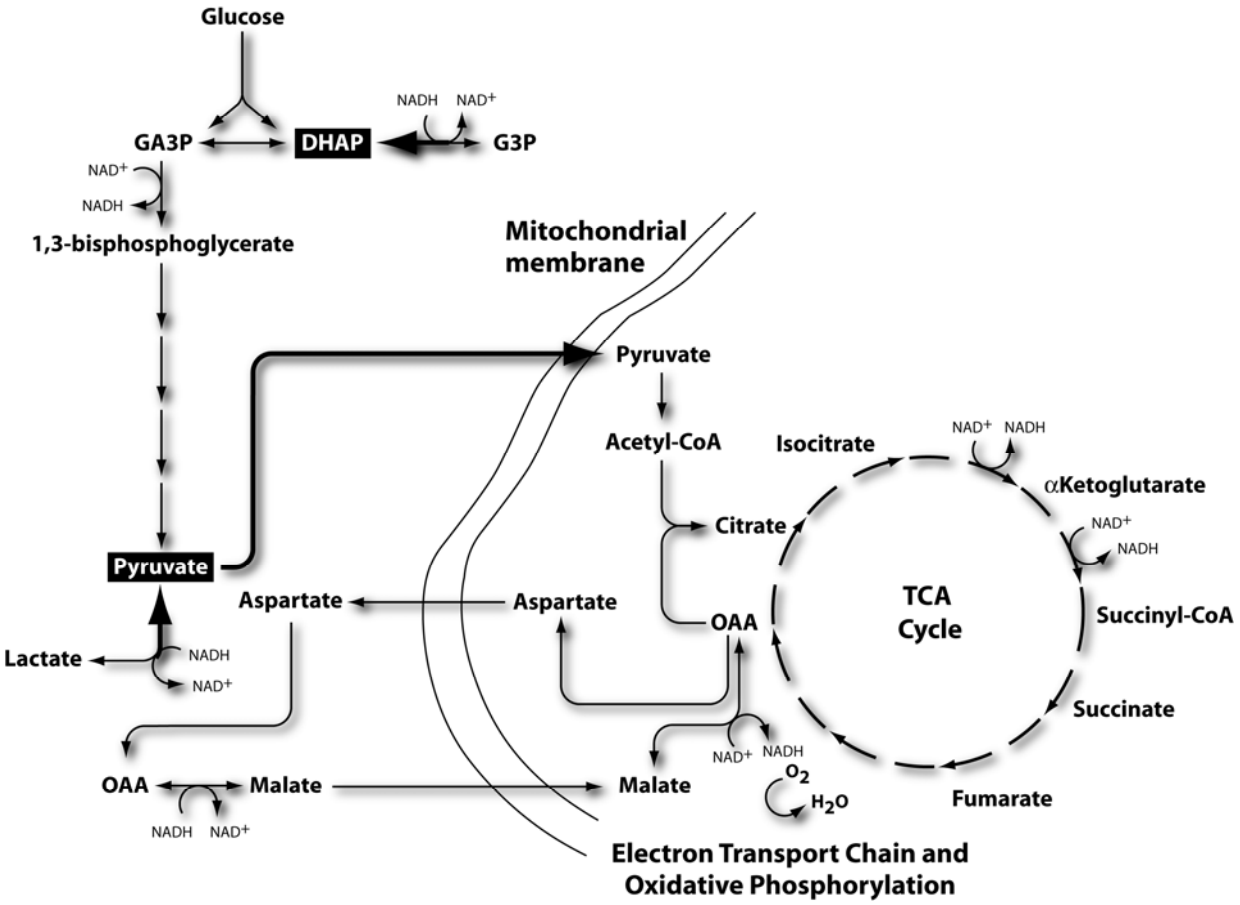
exposure groups. When ratios of G3P/DHAP and Lactate/Pyruvate are examined, both ratios are lower in 4.50 ATA O_2 group compared to the other 60 minute exposure groups (Figure 12). These metabolites are both involved in NAD^+ linked dehydrogenase reactions. A correlation to oxygen concentration can also be seen with the ratios (Figure 13) so the ratios seem to be linked to the concentration of oxygen. This can give insight into the equilibrium status of the dehydrogenase reaction. It shows that the 0.40 ATA O_2 group may be hypoxic. The lactate and G3P levels are elevated so the NAD^+/NADH ratio could be low (Figure 20).

Figure 20: Glycolytic pathway and TCA cycle affected by 0.40 ATA O_2.



This would agree with a study by Ben-Yoseph *et al.* that showed elevated G3P and NADH/NAD+ ratios in male Hartley guinea pig cerebral cortex slices exposed to severe hypoxia [44]. Also in the 4.50 ATA O_2 group, it shows that it is highly oxidized and there could be an elevated NAD+/NADH ratio. The cells may use oxidative phoshorylation and shuttle mechanisms from the cytosol to the mitochondrion to try to eliminate the toxic concentrations of oxygen by converting it to water within the electron transport chain. One such shuttle mechanism, the Malate-Aspartate Shuttle, uses NAD^+/NADH to transfer reducing equivalents from the cytosol to the mitochondrion (Figure 21). In the mitochondrion, this shuttle converts malate to oxaloacetate while NAD^+ is reduced to NADH. The reoxidation of NADH by the ETC allows the flow of electrons to drive ATP synthesis. In that process, O_2 get reduced to H_2O. This shuttle is considered the most important shuttle in the brain [45].

Figure 21: Glycolytic pathway and TCA cycle affected by 4.50 ATA O_2.



D. Phospholipid Synthesis and Degradation

By studying the peaks in the ^{31}P aqueous and lipid spectra, phospholipid synthesis and degradation pathways can be examined (Figure 17). Phosphoethanolamine (Petn) was found to be lower with increasing oxygen. There was significantly lower amount in the 4.50 ATA O_2 group than the 0.40 ATA O_2 group. A recent study showed that when high amounts of Petn are given exogenously to isolated mitochondria that electron transfer activity is inhibited [46]. So the increased amounts found in the 0.40 ATA O_2 group may impair mitochondrial function which may change slice metabolism. There were no differences in Glycerophosphoethanolamine (GPE) or Phosphatidylethanolamine

(PE) between groups. Since there were no other significant changes in these other lipids in the pathway, it could suggest that there is an effect on the lipid converting enzymes involved in the pathway, such as Ethanolamine kinase that converts ethanolamine to phosphoethanolamine or CTP: phosphoethanolamine cytidyl transferase that converts phosphoethanolamine to CDP-ethanolamine. Oxygen concentrations or ROS could have an effect on these enzymes although this has not been reported in the literature. It seems that PE biosynthesis is inhibited, but the PE concentration remains constant over all O_2 groups. PE can also be made by decarboxylation of PS, not just through the Kennedy pathway. There were no differences found in the phosphatidylcholine synthesis and degradation pathways though. Phosphatidylinositol (PI) and Cardiolipin (CL) were both found to be significantly lower in 4.50 ATA O_2 (Figure 18). Cardiolipin is primarily present in the inner mitochondrial membrane and very susceptible to peroxidation. Losses of cardiolipin in cultured rat neurons have been shown and those losses were due to oxidative damage caused by lipid peroxidation [47]. Morin et al. showed that ROS produced during *in vitro* reoxygenation studies of rat brain mitochondria is responsible for cardiolipin peroxidation [48]. The elevated oxygen concentrations may be causing peroxidation, which may lead to alterations in the mitochondria and how they function. A review of the role of cardiolipin in oxidative phosphorylation suggests that the headgroup may buffer protons in the electron transport chain (ETC) and may act as a regulator. This is so the ETC will not run out of control. This review suggests that when there is less cardiolipin that the basal metabolic rate increases [49] [50]. This may be why we also see increased levels of ATP in the 4.50 ATA O_2 group because there is less cardiolipin to regulate the ETC. There were no differences in PA or PE pls, which is

surprising knowing that it has been shown that plasmalogens can protect against an oxidative insult as shown in rat brain with phosphine-induced oxidative stress [39]. There was a trend that showed that PE pls and PA decreased with increasing oxygen concentration, although this was not significant (Table III).

E. Effects of Oxygen on Lipids

Lipids were also examined from the ^{13}C spectra (Figure 19). Cholesterol and triacylglycerides (TAG) showed a trend that with increasing oxygen there was less of each, although this was not significant. The Omega-3 FA was significantly lower when exposed to 4.50 ATA O_2 than with 0.40 ATA O_2. Both Omega-3 FA and cardiolipin are polyunsaturated fatty acids and were significantly lower in the 4.50 ATA O_2 group compared to the 0.40 ATA O_2 group. The increased amount of ROS at higher oxygen concentrations may cause lipid peroxidation and thus result in a lower amount of both of these lipids.

Metabolite ratios were compared between the 0.95 ATA O_2 group at 60 minutes and the 0.95 ATA O_2 group at 5 minutes (Table V). These were examined to see if there were differences over time instead of oxygen concentration. There was a significant increase in both lactate/pyruvate and G3P/DHAP over time. There is a shift in these metabolite ratios due to the oxidized forms of these metabolites being used to repair the cell membranes in the tissue slice. The Petn/PE, Petn/ PE pls, and Petn/GPE ratios all significantly decrease from the 5 minute to the 60 minute time point. It suggests that there is a loss of PE during slicing due to membrane rupture. The precursor in the biosynthetic pathway is Petn. Since there is a loss of PE the Petn/PE ratio is higher at 5

minutes than at 60 minutes when the membranes have repaired themselves. PE is also the precursor of PE pls and GPE. So the Petn/PE pls and Petn/GPE ratios are also lower at 60 minutes. By the 60 minute time point, the ratios are lower because the biosynthetic pathways are again using Petn for PE, PE pls, and GPE synthesis.

Chapter VI

Conclusions

These experiments have demonstrated that brain tissue slice metabolism can be affected by different doses of oxygen. They suggest that 0.40 ATA O_2 may make the tissue hypoxic and therefore shift metabolism toward anaerobic glycolysis to generate ATP. The reduced environment due to the low oxygen suggests a low NAD+/NADH which explains the elevated lactate and G3P. It also explains the low PCr/ATP. The elevated Petn could also inhibit electron transport activity to further reduce the energy status of the slices.

The results also suggest that high doses of oxygen may cause aerobic glycolysis and oxidative phosphorylation to accelerate. The environment is very oxidized which may mean an elevated NAD+/NADH and explains the lower lactate and G3P amounts and higher PCr/ATP ratio. The lower polyunsaturated FA amounts may be caused by increased ROS which may cause lipid peroxidation with cardiolipin and omega-3 FA. Lower cardiolipin amounts may cause the deregulation of the ETC. But the increase in superoxide shown by Dr. Dean and lower cardiolipin amounts found here suggest mitochondrial damage. The NAA amounts remained the same across all O_2 groups and suggest no neuronal damage and the energy status of the slices seems good. It may be very early damage and the effects have yet to fully develop.

The 0.40 ATA O_2 results suggest a hypoxic environment while the 0.95 and 4.50 ATA O_2 results suggest hyperoxic environments that lead to changes in metabolism on

both ends of the oxygen spectrum. These results suggest that an oxygen concentration between 0.40 ATA and 0.95 ATA for tissue slice work would reduce the changes in metabolism and mimic that which is found *in vivo.*

Chapter VII

References

1. Dean, J.B., et al., *Neuronal sensitivity to hyperoxia, hypercapnia, and inert gases at hyperbaric pressures.* J Appl Physiol, 2003. **95**(3): p. 883-909.
2. Cater DB, G.S., Marina F, and Silver IA, *Changes in oxygen tension in brain and somatic tissues induced by vasodilator and vasoconstrictor drugs.* Proc R Soc Lond B Biol Sci, 1961. **155**: p. 136-157.
3. Jamieson, D. and H.A. Vandenbrenk, *Measurement of Oxygen Tensions in Cerebral Tissues of Rats Exposed to High Pressures of Oxygen.* J Appl Physiol, 1963. **18**: p. 869-76.
4. McIlwain, H. and H.L. Buddle, *Techniques in tissue metabolism. I. A mechanical chopper.* Biochem J, 1953. **53**(3): p. 412-20.
5. Fujii, T., H. Baumgartl, and D.W. Lubbers, *Limiting section thickness of guinea pig olfactory cortical slices studied from tissue pO2 values and electrical activities.* Pflugers Arch, 1982. **393**(1): p. 83-7.
6. Mulkey, D.K., et al., *Oxygen measurements in brain stem slices exposed to normobaric hyperoxia and hyperbaric oxygen.* J Appl Physiol, 2001. **90**(5): p. 1887-99.
7. Emerit, J., M. Edeas, and F. Bricaire, *Neurodegenerative diseases and oxidative stress.* Biomed Pharmacother, 2004. **58**(1): p. 39-46.
8. Bickford, P.C., et al., *Effect of normobaric hyperoxia on two indexes of synaptic function in Fisher 344 rats.* Free Radic Biol Med, 1999. **26**(7-8): p. 817-24.
9. Demchenko, I.T., et al., *Oxygen seizure latency and peroxynitrite formation in mice lacking neuronal or endothelial nitric oxide synthases.* Neurosci Lett, 2003. **344**(1): p. 53-6.
10. Demchenko, I.T., et al., *Nitric oxide production is enhanced in rat brain before oxygen-induced convulsions.* Brain Res, 2001. **917**(2): p. 253-61.
11. Fessel J, A.W.C., Winder D, and Roberts LJ, *Standard brain slice protocols result in neruonal oxidative injury in hippocampal slices (Abstract).* Free Radic Biol Med, 2002. **33**: p. S433.
12. Torbati, D., et al., *Free radical generation in the brain precedes hyperbaric oxygen-induced convulsions.* Free Radic Biol Med, 1992. **13**(2): p. 101-6.
13. Droge, W., *Free radicals in the physiological control of cell function.* Physiol Rev, 2002. **82**(1): p. 47-95.
14. Elayan, I.M., et al., *Effect of hyperbaric oxygen treatment on nitric oxide and oxygen free radicals in rat brain.* J Neurophysiol, 2000. **83**(4): p. 2022-9.
15. Noda, Y., P.L. McGeer, and E.G. McGeer, *Lipid peroxide distribution in brain and the effect of hyperbaric oxygen.* J Neurochem, 1983. **40**(5): p. 1329-32.

16. Piantadosi, C.A. and L.G. Tatro, *Regional H2O2 concentration in rat brain after hyperoxic convulsions.* J Appl Physiol, 1990. **69**(5): p. 1761-6.
17. Jain, K., *Oxygen Toxicity*, in *Textbook of Hyperbaric Medicine*, J. KK, Editor. 1996, Hogrefe and Huber: Seattle. p. 63-78.
18. Pellmar, T., *Electrophysiological correlates of peroxide damage in guinea pig hippocampus in vitro.* Brain Res, 1986. **364**(2): p. 377-81.
19. Pellmar, T.C., *Use of brain slices in the study of free-radical actions.* J Neurosci Methods, 1995. **59**(1): p. 93-8.
20. Clark, J.a.T., SR, *Toxicity of oxygen, carbon dioxide, and carbon monoxide*, in *Bove and Davis' Diving Medicine*, A. Bove, Editor. 1997, Sauders: Philadelphia. p. 131-145.
21. Cragg, P.A., D.B. Drysdale, and J.H. Hamilton, *Ventilation in intact and glossopharyngeal nerve sectioned anaesthetized rats exposed to oxygen at high pressure.* J Physiol, 1986. **370**: p. 489-99.
22. Simon, A.J. and D. Torbati, *Effects of hyperbaric oxygen on heart, brain, and lung functions in rat.* Undersea Biomed Res, 1982. **9**(3): p. 263-75.
23. Torbati, D., A. Mokashi, and S. Lahiri, *Effects of acute hyperbaric oxygenation on respiratory control in cats.* J Appl Physiol, 1989. **67**(6): p. 2351-6.
24. Watanabe T, C.R., Dainer H, Dean JB, and Soutiere S, *Pre-ictal clinical manifestations in a swine model of hyperbaric oxygen-induced seizures (abstract).* Undersea and Hyperbaric Medicine, 2005.
25. Bindokas, V.P., et al., *Superoxide production in rat hippocampal neurons: selective imaging with hydroethidine.* J Neurosci, 1996. **16**(4): p. 1324-36.
26. Bourke, S., et al., *Development of a lung slice preparation for recording ion channel activity in alveolar epithelial type I cells.* Respir Res, 2005. **6**: p. 40.
27. Brewer, G.J. and C.W. Cotman, *Survival and growth of hippocampal neurons in defined medium at low density: advantages of a sandwich culture technique or low oxygen.* Brain Res, 1989. **494**(1): p. 65-74.
28. Mulkey, D.K., et al., *Oxidative stress decreases pHi and Na(+)/H(+) exchange and increases excitability of solitary complex neurons from rat brain slices.* Am J Physiol Cell Physiol, 2004. **286**(4): p. C940-51.
29. Mulkey, D.K., et al., *Hyperbaric oxygen and chemical oxidants stimulate CO2/H+-sensitive neurons in rat brain stem slices.* J Appl Physiol, 2003. **95**(3): p. 910-21.
30. D'Agostino, D.P., R.W. Putnam, and J.B. Dean, *Superoxide (*O2-) production in CA1 neurons of rat hippocampal slices exposed to graded levels of oxygen.* J Neurophysiol, 2007. **98**(2): p. 1030-41.
31. King, G.L. and J.L. Parmentier, *Oxygen toxicity of hippocampal tissue in vitro.* Brain Res, 1983. **260**(1): p. 139-42.
32. Wilson, C.L., et al., *Paired pulse suppression and facilitation in human epileptogenic hippocampal formation.* Epilepsy Res, 1998. **31**(3): p. 211-30.
33. Zhang, X., et al., *Gradation of kainic acid-induced rat limbic seizures and expression of hippocampal heat shock protein-70.* Eur J Neurosci, 1997. **9**(4): p. 760-9.

34. Garcia, A., III, Henderson RA III, and Dean JB, *Acute exposure to hyperbaric oxygen stimulates firing rate of CA1 neurons of the hippocampus (Abstract).* FASEB J, 2002. **16**: p. A1168.
35. Garcia, A., III, Henderson RA III, Putnam RW, and Dean JB, *Oxidative stress induced by hyperbaric oxygen increases the synaptic response of CA1 neurons in the rat hippocampus (Abstract).* FASEB J, 2003. **17**: p. A71.
36. Sunberg H, H.E., and Jellestad F, *Electrophysiological effects of hyperbaric oxygen exposure in freely moving rats*, in *Diving and Hyperbaric Medicine. Proceedings of the XIIIth Annual Meeting of the European Undersea Biomedical Society*, M.A.a.O. G, Editor. 1987, EUBS 87: Palermo. p. 141-147.
37. Reo, N.V., M. Adinehzadeh, and B.D. Foy, *Kinetic analyses of liver phosphatidylcholine and phosphatidylethanolamine biosynthesis using (13)C NMR spectroscopy.* Biochim Biophys Acta, 2002. **1580**(2-3): p. 171-88.
38. Reo, N.V. and M. Adinehzadeh, *NMR spectroscopic analyses of liver phosphatidylcholine and phosphatidylethanolamine biosynthesis in rats exposed to peroxisome proliferators-A class of nongenotoxic hepatocarcinogens.* Toxicol Appl Pharmacol, 2000. **164**(2): p. 113-26.
39. Kuczynski, B. and N.V. Reo, *Evidence that plasmalogen is protective against oxidative stress in the rat brain.* Neurochem Res, 2006. **31**(5): p. 639-56.
40. Jenkins, B.G., et al., *An integrated strategy for evaluation of metabolic and oxidative defects in neurodegenerative illness using magnetic resonance techniques.* Ann N Y Acad Sci, 1999. **893**: p. 214-42.
41. Hetherington, H.P., et al., *Quantitative (31)P spectroscopic imaging of human brain at 4 Tesla: assessment of gray and white matter differences of phosphocreatine and ATP.* Magn Reson Med, 2001. **45**(1): p. 46-52.
42. Sappey-Marinier, D., et al., *Phosphorus and proton magnetic resonance spectroscopy in episodic ataxia type 2.* Ann Neurol, 1999. **46**(2): p. 256-9.
43. Twieg, D.B., et al., *Phosphorus-31 magnetic resonance spectroscopy in humans by spectroscopic imaging: localized spectroscopy and metabolite imaging.* Magn Reson Med, 1989. **12**(3): p. 291-305.
44. Ben-Yoseph, O., et al., *Glycerol 3-phosphate and lactate as indicators of the cerebral cytoplasmic redox state in severe and mild hypoxia respectively: a 13C- and 31P-n.m.r. study.* Biochem J, 1993. **291 (Pt 3)**: p. 915-9.
45. McKenna, M.C., et al., *Neuronal and astrocytic shuttle mechanisms for cytosolic-mitochondrial transfer of reducing equivalents: current evidence and pharmacological tools.* Biochem Pharmacol, 2006. **71**(4): p. 399-407.
46. Modica-Napolitano, J.S. and P.F. Renshaw, *Ethanolamine and phosphoethanolamine inhibit mitochondrial function in vitro: implications for mitochondrial dysfunction hypothesis in depression and bipolar disorder.* Biol Psychiatry, 2004. **55**(3): p. 273-7.
47. Kirkland, R.A., et al., *Loss of cardiolipin and mitochondria during programmed neuronal death: evidence of a role for lipid peroxidation and autophagy.* Neuroscience, 2002. **115**(2): p. 587-602.
48. Morin, C., R. Zini, and J.P. Tillement, *Anoxia-reoxygenation-induced cytochrome c and cardiolipin release from rat brain mitochondria.* Biochem Biophys Res Commun, 2003. **307**(3): p. 477-82.

49. Haines, T.H. and N.A. Dencher, *Cardiolipin: a proton trap for oxidative phosphorylation.* FEBS Lett, 2002. **528**(1-3): p. 35-9.
50. Basova, L.V., et al., *Cardiolipin switch in mitochondria: shutting off the reduction of cytochrome c and turning on the peroxidase activity.* Biochemistry, 2007. **46**(11): p. 3423-34.

APPENDIX A

Quantitation Data Tables 60 Minute Timepoint					
Lipids from Carbon Spectra			n=5	n=6	n=6
	Signal PPM	**Saturation Factor**	**0.40 ATA**	**0.95 ATA 60 min**	**4.50 ATA**
			Mean ± SE	Mean ± SE	Mean ± SE
Chol C5 and C18	C5-141.3 C18-12.3	C5-0.064 C18-0.029	20.6 ± 1.8	19.33 ± 1.2	15.9 ± 1.5
w-3 C2	21	0.076	6.64 ± 0.74	5.72 ± 0.30	4.44 ± 0.51 *
TAG	69.1	0.038	3.63 ± 0.57	2.72 ± 0.28	2.34 ± 0.37
Chol C6	122.1	0.024	16.31±1.75	16.14±1.09	13.06±1.07
PC	54.4	0.024	11.77±1.27	10.84±0.58	8.93±0.78
Phospholipids			n=5	n=6	n=6
			0.40 ATA	**0.95 ATA 60 min**	**4.50 ATA**
PC	-0.84	0.024	11.77±1.27	10.84±0.58	8.93±0.78
PE	0.02		5.2±0.58	4.84±0.30	4.07±0.42
PS	-0.18		3.32±0.36	2.99±0.19	2.52±0.27
SM	-0.06		1.13±0.11	1.03±0.07	0.90±0.10
Choline Pls	-0.78		0.27±0.05	0.24±0.02	0.25±0.05
unknown	0.12		0.23±0.06	0.22±0.02	0.15±0.02
PE pls	0.08		7.23 ± 0.76	6.40 ± 0.35	5.24 ± 0.45
PI	-0.4		0.70 ± 0.09	0.55 ± 0.04	0.44 ± 0.06 *
CL	0.16		0.53 ± 0.08	0.48 ± 0.03	0.32 ± 0.03 *
PA	0.22		0.35 ± 0.05	0.29 ± 0.02	0.22 ± 0.02

* denotes significant difference from 0.40 ATA O_2 (ANOVA, Tukey HSD $p \leq .05$)

Quantitation Data Tables 60 Minute Timepoint					
Metabolites from Proton Aqueous Spectra			n=6	n=6	n=6
	Signal PPM	**Saturation Factor**	**0.40 ATA**	**0.95 ATA 60 min**	**4.50 ATA**
NAA	4.4		4.60 ± 0.53	3.74 ± 0.22	4.16 ± 0.52
Myo-inositol	4.04		4.16±0.49	3.44±0.26	3.33±0.39
Cr & PCr	3.96		5.53 ± 0.67	4.73 ± 0.21	4.90 ± 0.52
Aspartate	3.88		1.03±0.13	0.98±0.09	1.07±0.15
Pyruvate	2.36		.88 ± 0.12	0.76 ± 0.06	1.03 ± 0.12
Acetate	1.88		1.73 ± 0.20	1.25 ± 0.09	0.96 ± 0.08 *
Lactate	4.12		12.14 ± 1.7	8.26 ± 0.95	3.37 ± 0.45 ‡
Metabolites from Phosphorus Aqueous Spectra			n=5	n=6	n=6
			0.40 ATA	**0.95 ATA 60 min**	**4.50 ATA**
DHAP	7.9	1.071	0.12 ± 0.02	0.12 ± 0.01	0.12 ± 0.04
G3P	7.5	1.061	0.50 ± 0.03	0.44 ± 0.06	0.10 ± 0.01 ‡
ATP	-18.2	0.723	0.39 ± 0.03	0.36 ± 0.04	0.51 ± 0.05
PCr	0	0.815	0.43 ± 0.06	0.59 ± 0.07	1.08 ± 0.12 ‡
Petn	6.9	0.736	0.23 ± 0.01	0.10 ± 0.05	0.08 ± 0.03 *
Pcho	6.5	1.064	0.18 ± 0.2	0.19 ± 0.02	0.16 ± 0.01
GPE	3.7	1.737	0.18 ± 0.02	0.20 ± 0.01	0.20 ± 0.02
GPC	3	1.08	0.25 ± 0.02	0.29 ± 0.02	0.32 ± 0.03
NAD(H)	-8.5	0.402	0.06 ± 0.0	0.06 ± 0.01	0.06 ± 0.01
Pi	5.5	1.691	4.15 ± 0.26	4.62 ± 0.39	3.50 ± 0.31

* denotes significant difference from 0.40 ATA O_2 (ANOVA, Tukey HSD $p \leq .05$)

‡ denotes significant difference from 0.40 and 0.95 ATA O_2 (ANOVA, Tukey HSD $p \leq .05$)

Ratios 60 Minute Timepoint			
Ratios	n=6	n=6	n=6
	0.40 ATA	**0.95 ATA 60 min**	**4.50 ATA**
NAA/Creatine	0.40±0.01	0.39±0.01	0.39±0.01
Lactate/Creatine	1.03±0.05	0.84±0.08	0.38±0.05
Myo-inositol/Creatine	0.35±0.01	0.34±0.02	0.31±0.01
Lactate/Pyruvate	4.36 ± 0.30	3.62 ± 0.30	1.26 ± 0.12 ‡
Pyruvate/Creatine	0.22±0.01	0.23±0.01	0.29±0.02
PCr/ATP	1.12 ± 0.12§	1.66 ± 0.16	2.11 ± 0.13
ATP/Pi	0.09 ± 0.01	0.08 ± 0.01	0.15 ± 0.02 ‡
G3P/DHAP	5.08 ± 0.85	3.61 ± 0.38	0.94 ± 0.13 ‡
Petn/PE	6.35 ± 0.76	8.50 ± 1.50	11.13 ± 1.76
Petn/PE Pls	4.57 ± 0.56	6.34 ± 1.04	8.48 ± 1.25
Petn/GPE	0.08 ± 0.01	0.12 ± 0.02	0.15 ± 0.02

‡ denotes significant difference from 0.40 and 0.95 ATA O_2 (ANOVA, Tukey HSD $p \leq .05$)

§ denotes significant difference from 0.95 and 4.50 ATA O_2 (ANOVA, Tukey HSD $p \leq .05$)

APPENDIX B

Quantitation Data Tables 0.95 ATA 5 and 60 Minute Timepoints				
Lipids from Carbon Spectra			n=4	n=6
	Signal PPM	**Saturation Factor**	**0.95 ATA 5 min**	**0.95 ATA 60 min**
			Mean ± SE	Mean ± SE
Chol C5 and C18	C5-141.3 C18- 12.3	C5-0.064 C18-0.029	17.62 ± 1.2	19.33 ± 1.2
w-3 C2	21	0.076	5.48 ± 0.50	5.72 ± 0.30
TAG	69.1	0.038	2.44 ± 0.19	2.72 ± 0.28
Chol C6	122.1	0.024	14.04±0.93	16.14±1.09
PC	54.4	0.024	9.80±0.59	10.84±0.58
Phospholipids			n=4	n=6
			0.95 ATA 5 min	**0.95 ATA 60 min**
PC	-0.84	0.024	9.80±0.59	10.84±0.58
PE	0.02		4.24±0.23	4.84±0.30
PS	-0.18		2.74±0.13	2.99±0.19
SM	-0.06		0.97±0.03	1.03±0.07
Choline Pls	-0.78		0.28±0.01	0.24±0.02
unknown	0.12		0.25±0.05	0.22±0.02
PE pls	0.08		5.85 ± 0.38	6.40 ± 0.35
PI	-0.4		0.48 ± 0.03	0.55 ± 0.04
CL	0.16		0.47 ± 0.05	0.48 ± 0.03
PA	0.22		0.27 ± 0.02	0.29 ± 0.02

Quantitation Data Tables 0.95 ATA 5 and 60 Minute Timepoints				
Metabolites from Proton Aqueous Spectra			n=4	n=6
	Signal PPM	**Saturation Factor**	**0.95 ATA 5 min**	**0.95 ATA 60 min**
NAA	4.4		4.83 ± 0.41	3.74 ± 0.22 ¥
Myo-inositol	4.04		4.21±0.21	3.44±0.26
Cr & PCr	3.96		5.68 ± 0.41	4.73 ± 0.21
Aspartate	3.88		1.37±0.06	0.98±0.09
Pyruvate	2.36		1.28 ± 0.08	0.76 ± 0.06 ¥
Acetate	1.88		1.00 ± 0.04	1.25 ± 0.09
Lactate	4.12		7.42 ± 0.88	8.26 ± 0.95
Metabolites from Phosphorus Aqueous Spectra			n=4	n=6
			0.95 ATA 5 min	**0.95 ATA 60 min**
DHAP	7.9	1.071	0.15 ± 0.03	0.12 ± 0.01
G3P	7.5	1.061	0.18 ± 0.03	0.44 ± 0.06 ¥
ATP	-18.2	0.723	0.29 ± 0.05	0.36 ± 0.04
PCr	0	0.815	0.60 ± 0.09	0.59 ± 0.07
Petn	6.9	0.736	0.05 ± 0.01	0.10 ± 0.05
Pcho	6.5	1.064	0.16 ± 0.02	0.19 ± 0.02
GPE	3.7	1.737	0.21 ± 0.02	0.20 ± 0.01
GPC	3	1.08	0.27 ± 0.03	0.29 ± 0.02
NAD(H)	-8.5	0.402	0.06 ± 0.01	0.06 ± 0.01
Pi	5.5	1.691	5.19 ± 0.56	4.62 ± 0.39

¥ denotes significant difference from 0.95 ATA O_2 at 5 min (ANOVA, Tukey HSD $p \leq .05$)

Quantitation Data Tables 0.95 ATA 5 and 60 Minute Timepoints		
Ratios	n=4	n=6
	0.95 ATA 5 min	**0.95 ATA 60 min**
NAA/Creatine	0.38±0.0	0.39±0.01
Lactate/Creatine	0.6±0.05	0.84±0.08
Myo-inositol/Creatine	0.33±0.01	0.34±0.02
Lactate/Pyruvate	1.88 ± 0.15	3.62 ± 0.30 ¥
Pyruvate/Creatine	0.31±0.0	0.23±0.01
PCr/ATP	2.08 ± 0.20	1.66 ± 0.16
ATP/Pi	0.06 ± 0.01	0.08 ± 0.01
G3P/DHAP	1.30 ± 0.21	3.61 ± 0.38 ¥
Petn/PE	20.04 ± 0.34	8.50 ± 1.50 ¥
Petn/PE Pls	14.56 ± 0.29	6.34 ± 1.04 ¥
Petn/GPE	0.26 ± 0.01	0.12 ± 0.02 ¥

¥ denotes significant difference from 0.95 ATA O_2 at 5 min (ANOVA, Tukey HSD $p \leq .05$)